

## RESEARCH ARTICLE

10.1002/2014JB011845

## Key Points:

- An improved inversion algorithm for deformation data is developed
- The stress exponent for olivine is more variable than previously thought
- This study undermines the previous multiscale modeling of seismic anisotropy

## Correspondence to:

J. Korenaga,  
jun.korenaga@yale.edu

## Citation:

Mullet, B. G., J. Korenaga, and S.-I. Karato (2015), Markov chain Monte Carlo inversion for the rheology of olivine single crystals, *J. Geophys. Res. Solid Earth*, 120, 3142–3172, doi:10.1002/2014JB011845.

Received 16 DEC 2014

Accepted 11 MAR 2015

Accepted article online 16 MAR 2015

Published online 27 MAY 2015

## Markov chain Monte Carlo inversion for the rheology of olivine single crystals

Benjamin G. Mullet<sup>1</sup>, Jun Korenaga<sup>1</sup>, and Shun-Ichiro Karato<sup>1</sup><sup>1</sup>Department of Geology and Geophysics, Yale University, New Haven, Connecticut, USA

**Abstract** We present major modifications to the Markov chain Monte Carlo inversion method of Korenaga and Karato (2008), which was developed to analyze rock deformation data and determine a corresponding flow law and its uncertainty. The uncertainties of state variables, e.g., temperature, pressure, and stress, are now taken into account by data randomization, to avoid parameter bias that could be introduced by the original implementation of the cost function. Also, it is now possible to handle a flow law composed of both parallel and sequential deformation mechanisms, by using conjugate gradient search to determine scaling constants. We test the new inversion algorithm extensively using synthetic data as well as the high-quality experimental data of Bai et al. (1991) on the deformation of olivine single crystals. Our reanalysis of this experimental data set reveals that a commonly adopted value for the stress exponent (~3.5) is considerably less certain than previously reported, and we offer a detailed account for the validity of our new estimates. The significance of fully reporting parameter uncertainties including covariance is also discussed with a worked example on flow law prediction under geological conditions.

## 1. Introduction

The rheology of silicate minerals is of fundamental importance for mantle dynamics, as it dictates how mantle materials respond to applied stress under various thermodynamic conditions [Karato and Wu, 1993; Kohlstedt et al., 1995; Hirth and Kohlstedt, 2003; Karato, 2008]. Laboratory experiments on the deformation of single crystals and mineral aggregates are the primary source of constraints on rheological parameters [e.g., Chopra and Paterson, 1984; Karato et al., 1986; Bai et al., 1991; Hirth and Kohlstedt, 1995b; Mei and Kohlstedt, 2000; Karato and Jung, 2003; Chen et al., 2006; Nishihara et al., 2008; Hansen et al., 2011], though additional insight can be brought from field observations as well [e.g., Jin et al., 1998; Warren and Hirth, 2006; Skemer et al., 2013].

The rheology of a given system, either a single crystal or a mineral aggregate, is usually described by a flow law or a set of flow laws, in which a strain rate is expressed as a function of stress and other state variables such as temperature and pressure. Estimating flow law parameters, e.g., a stress exponent and an activation energy, from deformation data is a complex nonlinear inverse problem, though experimentalists have long adopted approximate treatments, for the sake of simplicity as well as tractability.

Korenaga and Karato [2008, hereinafter referred to as KK08] attempted to construct a rigorous theoretical framework for the analysis of deformation data, based on Bayesian statistics using a Markov chain Monte Carlo (MCMC) method. This initiative left some room for improvement. First, KK08 applied their MCMC code to the composite rheology of olivine aggregates, without documenting any benchmark test of the code. The absence of reported benchmark tests, combined with the complexity of the composite rheology investigated, made the understanding of how the new approach works more difficult than necessary. Second, we later realized that the original MCMC implementation was not optimal in handling data uncertainty. The cost function was formulated to take into account the uncertainties of all state variables, but the direct use of this cost function in MCMC sampling could potentially introduce some parameter bias. MCMC-based inversion for rheological parameters is still very time-consuming, so it may not become a standard tool for experimentalists anytime soon. Nevertheless, it is important to demonstrate the benefit of adopting the comprehensive statistical approach with an improved algorithm.

The purpose of this study is thus twofold. First, we report two major modifications made for the original implementation of KK08. To minimize unwanted parameter bias, data uncertainty is now incorporated by the technique of data randomization. The original MCMC code was also modified to be more flexible to handle both parallel and sequential combinations of flow laws. Second, we apply the revised MCMC

**Table 1.** Notation

Variable	Meaning	Units
$M$	the number of experimental runs	
$N_m$	the number of experiments in $m$ th run	
$\dot{\epsilon}_{\text{obs}}^{j_m}$	strain rate for $j_m$ th experiment in $m$ th run	$\text{s}^{-1}$
$\{s_l^m\}$	a set of other state variables for $j_m$ th experiment	
$\sigma$	stress	MPa
$f_{\text{O}_2}$	oxygen fugacity	atm
$T$	temperature	K
$\{q_k\}$	a set of flow law parameters	
$N_p$	the number of parallel mechanisms	
$N_s$	the number of sequential mechanisms	
$A_i$	scaling constant for $i$ th deformation mechanism	
$B_i$	normalized scaling constant for $i$ th mechanism	
$n_i$	stress exponent for $i$ th deformation mechanism	
$m_i$	oxygen fugacity exponent for $i$ th deformation mechanism	
$Q_i$	activation enthalpy for $i$ th deformation mechanism	$\text{J mol}^{-1}$
$X_m$	interrun bias parameter for $m$ th run	
$K$	the total number of parameters to be estimated	
$D$	the iteration interval for data randomization	
$P$	the number of trials in Gibbs sampling	
$C$	the number of initial guesses in conjugate gradient search	

approach to the deformation data of olivine single crystals, to provide a variety of inversion examples. We use the high-quality experimental data of *Bai et al.* [1991, hereinafter referred to as BMK91], the comprehensive nature of which allows us to conduct both simple and complex inversions. A comparison between our inversion results and theirs serves to elucidate potential pitfalls in the standard procedure adopted by experimentalists.

The structure of this paper is as follows. The revised MCMC algorithm is first described with a relevant theoretical background. Then, after briefly summarizing the experimental data of BMK91, inversion results are

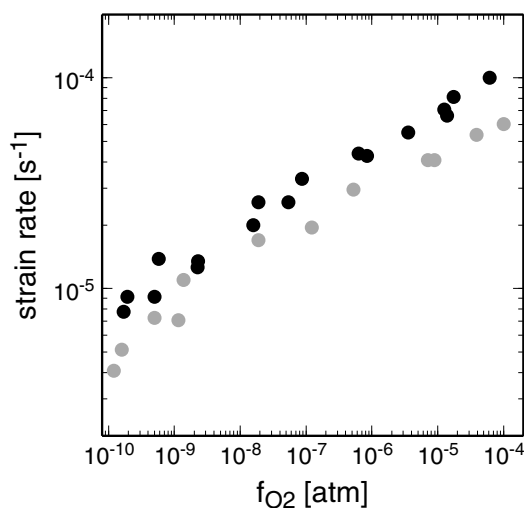


**Figure 1.** Raw deformation data for runs 5207 (solid) and 5215 (gray) for  $[101]_c$  with opx buffer [Bai, 1990]. These two runs were conducted under the same temperature (1673 K) and stress (30 MPa), so the systematic difference between them indicates the presence of an interrune bias.

presented for individual experimental runs. At this point, there is no significant difference between our results and the original results of BMK91. Critical difference arises when we conduct global inversion by assembling different experimental runs. We offer an explanation for the difference and also point out the importance of parameter covariance. A worked example is given to illustrate how to use the new inversion results, and the paper is closed with some remarks on possible future directions. The benchmark tests of the new MCMC code using synthetic data are reported in appendix.

## 2. Theoretical Framework

### 2.1. Error Propagation With Data Randomization

As in KK08, we use the following statistical model for measured strain rate data:

$$\dot{\epsilon}_{\text{obs}}^j = \dot{\epsilon} \left( \{q_k\}; \{s_l^j\} \right) \exp(X), \quad (1)$$

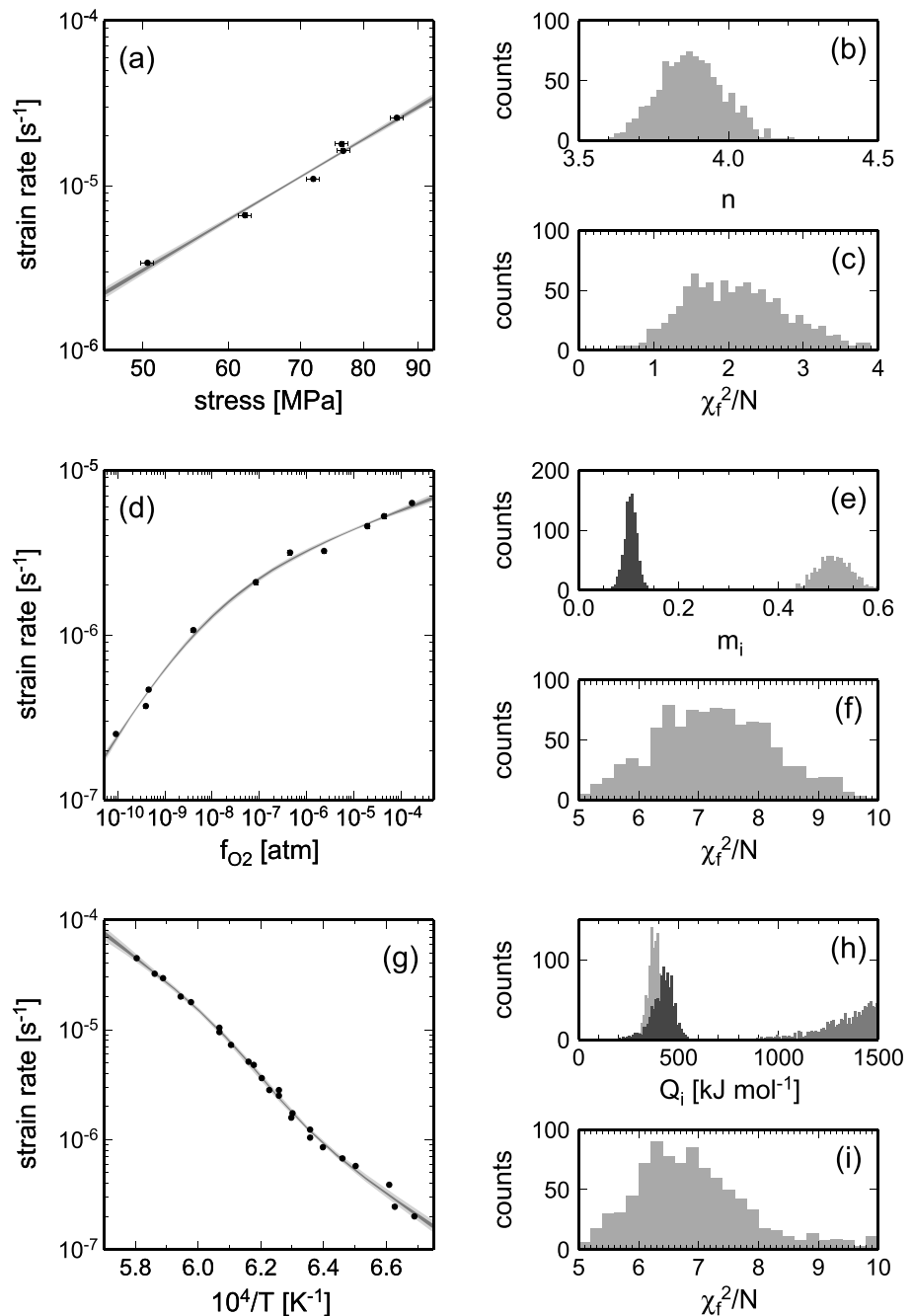


**Figure 2.** Example of single-run inversion results. (a, d, g) Experimental data are compared with 50% (dark gray) and 90% (light gray) confidence limits based on MCMC ensemble, and (b, e, h) the distributions of flow law parameters and (c, f, i) normalized  $\chi_f^2$  are shown. Figures 2a–2c are for run 7602 ([101]<sub>c</sub> with mw buffer,  $T = 1673$  K, and  $f_{O_2} = 3.2 \times 10^{-10}$  atm), and the key parameter is the stress exponent  $n$ , Figures 2d–2f for run 5202 ([101]<sub>c</sub> with opx buffer,  $T = 1673$  K and  $\sigma = 30$  MPa), with the fugacity exponents  $m_1$  (light gray) and  $m_2$  (dark gray), and Figures 2g–2i for run 7205 ([110]<sub>c</sub> with opx buffer,  $\sigma = 40$  MPa and  $f_{O_2} = 2.5 \times 10^{-7}$  atm), with the activation enthalpies  $Q_1$  (light gray),  $Q_2$  (medium gray), and  $Q_3$  (dark gray).

where  $\dot{\epsilon}_{obs}^j$  is a strain rate for  $j$ th experiment in a particular run,  $\{q_k\}$  is a set of flow law parameters,  $\{s_j^i\}$  is a set of relevant state variables such as temperature and stress,  $\dot{\epsilon}(\{q_k\}; \{s_j^i\})$  is a corresponding theoretical prediction, and  $X$  is a random variable. The term  $\exp(X)$  represents a bias of this run with respect to some reference run and is meant to absorb collectively all kinds of unprescribed uncertainties that stay largely constant during an individual run.

Our task is to find a set of flow law parameters that can explain all strain rate measurements within experimental uncertainties. KK08 used the following cost function to quantify the success of a given set of flow law parameters:

$$\chi_f^2(\{q_k\}, \{X_m\}) = \sum_{m=1}^M \sum_{j_m=1}^{N_m} \frac{(\log \dot{\epsilon}_{\text{obs}}^{j_m} - \log \dot{\epsilon}(\{q_k\}; \{s_l^{j_m}\}) - X_m)^2}{\text{rvar}(\dot{\epsilon}^{j_m}) + \text{rvar}(\{q_k\}; \{s_l^{j_m}\})}, \quad (2)$$

where  $M$  is the number of experimental runs,  $N_m$  is the number of data in the  $m$ th run,  $\text{rvar}(\dot{\epsilon}^{j_m})$  denotes a relative variance of strain rate, and  $\text{rvar}(\{q_k\}; \{s_l^{j_m}\})$  denotes a relative variance introduced by the uncertainty of other state variables (see Appendix A). Whereas the above cost function takes into account the uncertainty of all relevant state variables, the second relative variance term,  $\text{rvar}(\{q_k\}; \{s_l^{j_m}\})$ , depends not only on  $\{s_l^{j_m}\}$  but also on  $\{q_k\}$ , and in general, the relative variance is greater for larger values of  $\{q_k\}$ . It is possible, therefore, to reduce the cost function not by minimizing the difference between observed and predicted strain rates but by increasing the second relative variance with larger flow law parameter values. For example, if a stress exponent can vary from 3 to 5 without affecting data misfit much, an MCMC search would preferentially sample values close to 5 because the cost function is lower for a higher exponent. Directly minimizing this cost function thus has a danger of introducing parameter bias.

In this paper, we propose to minimize the following simpler cost function:

$$\chi^2(\{q_k\}, \{X_m\}) = \sum_{m=1}^M \sum_{j_m=1}^{N_m} \frac{(\log \dot{\epsilon}_{\text{obs}}^{j_m} - \log \dot{\epsilon}(\{q_k\}; \{s_l^{j_m}\}) - X_m)^2}{\text{rvar}(\dot{\epsilon}^{j_m})}, \quad (3)$$

which lacks the second variance term in the denominator. To compensate for this, we propagate the uncertainty of state variables into that of flow law parameters, by randomly perturbing experimental data within their uncertainties. Error propagation by data randomization is a standard technique in Monte Carlo error analysis [e.g., *Robert and Casella, 2004*], and in our case, it helps to prevent parameter bias by simplifying the cost function to be minimized. The full cost function of equation (2) is still useful to evaluate the misfit between observed and predicted strain rates by taking into account all relevant uncertainties, and we will calculate it in addition to the new cost function; an important aspect is that the full cost function is no longer the target of minimization.

## 2.2. Flow Law Scaling With Conjugate Gradient Search

The MCMC code developed by KK08 was revised to handle the following form of a theoretical flow law:

$$\dot{\epsilon}(\{q_k\}; \{s_l\}) = \sum_{i_p=1}^{N_p} A_{i_p} \sigma^{n_{i_p}} f_{O_2}^{m_{i_p}} \exp\left(\frac{Q_{i_p}}{RT}\right) + \left[ \sum_{i_s=1}^{N_s} \left( A_{i_s} \sigma^{n_{i_s}} f_{O_2}^{m_{i_s}} \exp\left(\frac{Q_{i_s}}{RT}\right) \right)^{-1} \right]^{-1}, \quad (4)$$

where  $N_p$  and  $N_s$  are, respectively, the number of parallel and sequential mechanisms,  $A_i$  is a scaling constant,  $\sigma$  is stress in MPa,  $n$  is the stress exponent,  $f_{O_2}$  is oxygen fugacity in atm,  $m$  is the oxygen fugacity exponent,  $Q$  is the activation enthalpy,  $R$  is the universal gas constant, and  $T$  is the absolute temperature. A set of flow law parameters  $\{q_k\}$  consists of  $A_{i_p}$ ,  $n_{i_p}$ ,  $m_{i_p}$ , and  $Q_{i_p}$  with  $i_p = 1, 2, \dots, N_p$  and  $A_{i_s}$ ,  $n_{i_s}$ ,  $m_{i_s}$ ,  $Q_{i_s}$  with  $i_s = 1, 2, \dots, N_s$ . A set of state variables  $\{s_l\}$  includes  $\sigma$ ,  $f_{O_2}$ , and  $T$ . Note that the interrurn bias parameter  $X_m$ , which can vary among different experimental runs, is not part of the theoretical flow law. See Table 1 for the list of variables used in this paper.

As noted by KK08, a bottleneck in the application of the MCMC strategy to the estimation of flow law parameters lies in scaling constants. To build an efficient MCMC algorithm, these constants should be treated differently from other flow-law parameters because of the absence of a priori bounds. The fast determination method for scaling constants devised by KK08 can be applied only to the combination of parallel mechanisms, so we have implemented a conjugate gradient search to determine scaling constants for a given set of other flow law parameters. The new approach is found to be about 10 times slower when only parallel mechanisms exist, but it is the only practical way to handle more complex situations. As a conjugate gradient search could be trapped in local minima, we use multiple initial guesses and choose a search result with the smallest value of the cost function.

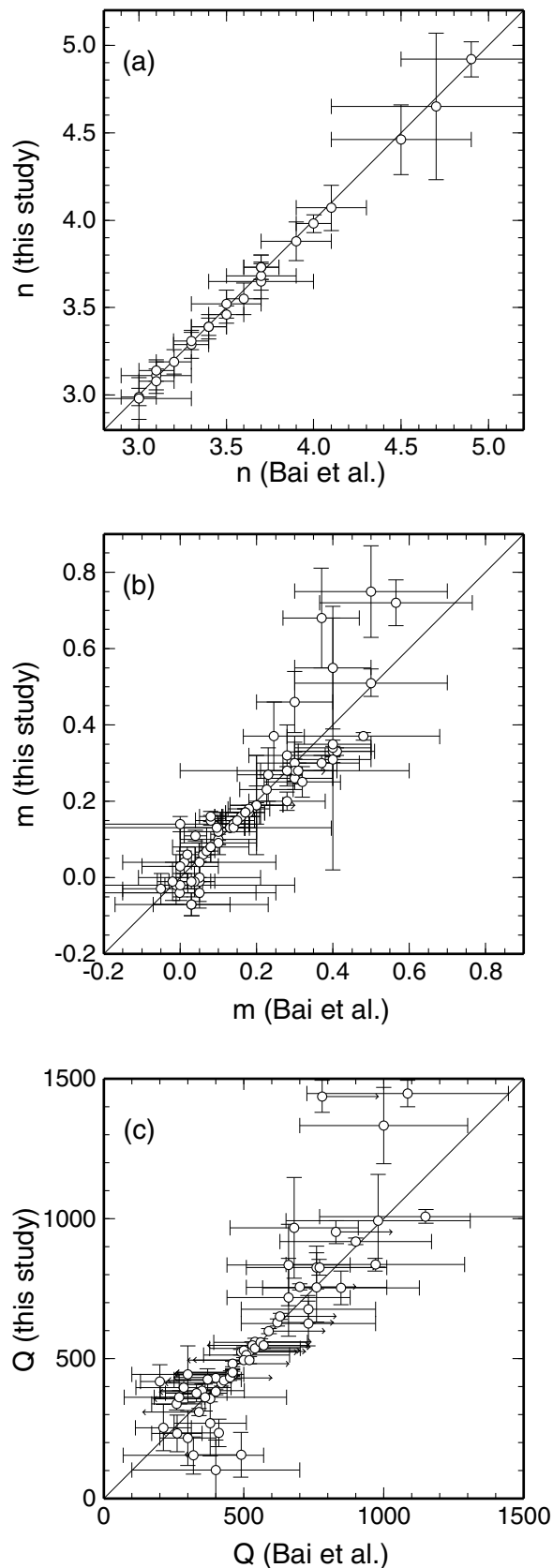


**Figure 3.** Comparison of single-run inversion results with those of BMK91 for (a) the stress exponents, (b) the oxygen fugacity exponents, and (c) the activation enthalpies. Error bars denote  $1\sigma$ .

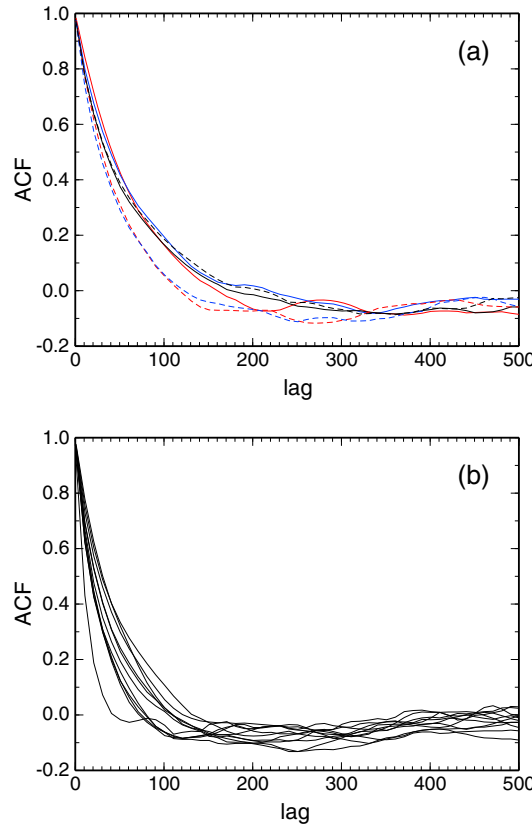


**Figure 4.** Autocorrelation function (ACF) for one of MCMC runs for the case of [011]<sub>c</sub> with mw buffer. (a) ACFs for flow law parameters,  $n_1$  (red),  $Q_1$  (blue),  $m_1$  (black),  $n_2$  (red, dashed),  $Q_2$  (blue, dashed), and  $m_2$  (black, dashed). (b) ACFs for 11 interrurn biases.

**2.3. Revised MCMC Procedure**

The MCMC algorithm that incorporates the aforementioned modifications may be summarized as follows:

1. *Initialization.* Draw  $K$  random numbers,  $r_k$ , from the interval  $[0,1]$  to set the initial model as

$$\{q_k^0\} = \{q_1^0, q_2^0, \dots, q_K^0\}, \quad (5)$$

where  $q_k^0 = q_k^l + r_k(q_k^u - q_k^l)$  for  $k = 1, 2, \dots, K$ . Here  $K$  is the total number of parameters to be estimated. Whereas  $\{q_k\}$  in equations (1)–(4) includes scaling constants but excludes inter-run biases, it is used here to denote all of flow law parameters except for scaling constants as well as interrurn biases. This is because scaling constants are not directly sampled by MCMC and because interrurn biases have to be estimated simultaneously with flow law parameters. The a priori lower and upper bounds on  $q_k$  are denoted by  $q_k^l$  and  $q_k^u$ , respectively. Set the iteration counter to 0.

2. *Data Randomization.* If the iteration counter is a multiple of some prescribed integer,  $D$ , randomize all experimental data within their uncertainties. Otherwise, use the same data from the previous iteration.

3. *Random Scan.* Pick one model parameter randomly from  $\{q_k | k = 1, 2, \dots, K\}$  and call it  $q_r$ . The random-scan Gibbs sampling requires an estimate on the following conditional likelihood:

$$L(\{q_1^n, \dots, q_{r-1}^n, q_r, q_{r+1}^n, \dots, q_K^n\}; \{A_i\}), \quad (6)$$

where the superscript  $n$  denotes the iteration counter (not the power), so we draw  $P$  random numbers from the interval  $[q_r^l, q_r^u]$  and calculate corresponding likelihood values. The likelihood is calculated from the cost function as

$$L(\{q_k\}; \{A_i\}) = \exp\left(-\frac{1}{2}\chi^2(\{q_k\}; \{A_i\})\right), \quad (7)$$

where scaling constants  $\{A_i\}$  are determined by a conjugate gradient search with  $C$  initial guesses (section 2.2). With a sufficiently large  $P$ , the conditional likelihood function can be approximated by the rejection sampling. Save the highest likelihood as  $L_{\max}$ .

4. *Gibbs Sampling.* Pick one random number from the interval  $[q_r^l, q_r^u]$  and call it  $q'_r$ . Construct a trial model:

$$\{q'_k\} = \{q_1^n, \dots, q_{r-1}^n, q'_r, q_{r+1}^n, \dots, q_K^n\}, \quad (8)$$

and calculate  $L(\{q'_k\}; \{A_i\})$ . Draw one more random number,  $s$ , from the interval  $[0,1]$ .

If  $s < L(\{q'_k\}; \{A_i\})/L_{\max}$ , go to the next step. Otherwise, start over this step.

5. *Model Update.* Calculate  $\chi^2(\{q_k^n\}; \{A_i\})$  for the old model and define the new model with  $\{q'_k\}$ , i.e.,

$$\{q_k^{n+1}\} = \{q_1^n, \dots, q_{r-1}^n, q'_r, q_{r+1}^n, \dots, q_K^n\}. \quad (9)$$

Until the maximum number of iterations is reached, increment the counter by one and go back to step 2.

Because the random-scan Gibbs sampling perturbs only one parameter at each iteration, the ensemble of saved models is highly correlated to each other. It is thus necessary to resample the ensemble at a sufficiently long interval to obtain a collection of statistically independent models. A proper resampling interval

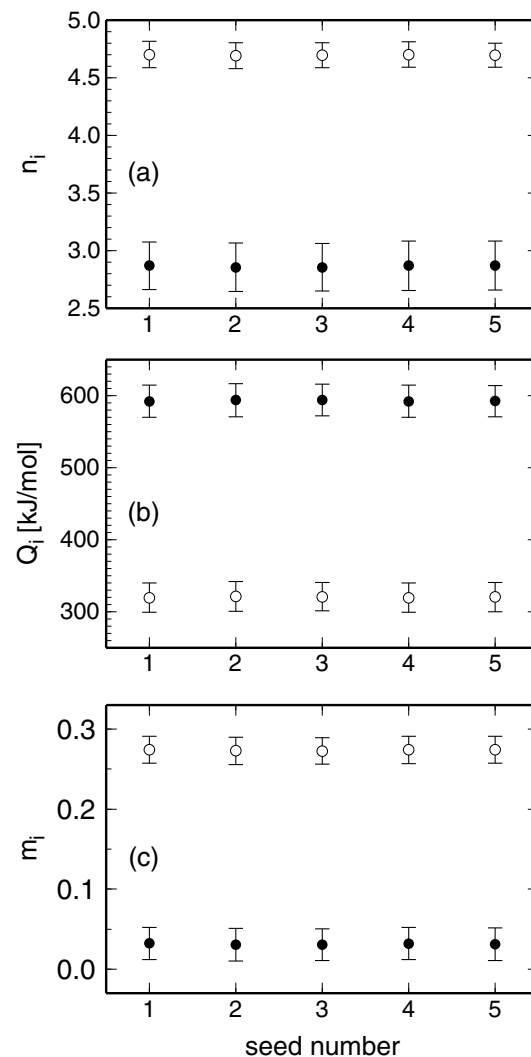


**Figure 5.** Comparison of results from five parallel MCMC runs for the case of  $[101]_c$  with opx buffer, in terms of mean and standard deviation: (a) the stress exponents  $n_1$  (open) and  $n_2$  (solid), (b) the activation enthalpies  $Q_1$  (open) and  $Q_2$  (solid), and (c) the oxygen fugacity exponents  $m_1$  (open) and  $m_2$  (solid).

Among six different combinations of buffer and orientation, BMK91 found that four cases ( $[101]_c$  with opx buffer, and  $[101]_c$ ,  $[011]_c$ , and  $[110]_c$  with mw buffer) can be explained by equation (4) with  $N_p = 0$  and  $N_s = 2$  (i.e., sequential mechanisms only), the case of  $[011]_c$  with opx buffer by  $N_p = 2$  and  $N_s = 0$  (parallel mechanisms only), and the case of  $[110]_c$  with opx buffer by  $N_p = 1$  and  $N_s = 2$  (mixture of parallel and sequential mechanisms). Revisiting the analysis of BMK91 thus provides an opportunity to test the revised MCMC code extensively.

The uncertainty of temperature was reported by BMK91 as  $\pm 1$  K, but other experimental uncertainties were not documented, so they are supplemented as follows (D. L. Kohlstedt, personal communication, 2014): the load and area were both known to within 1%, amounting to  $\sim 1.4\%$  uncertainty of applied stress. The displacement of the sample was known to within 3%, and time is virtually error free, so the relative uncertainty of strain rate is 3%. The oxygen fugacity was known to within 2%. Our data randomization is conducted with these uncertainties.

The uncertainties that are more difficult to deal with include those related to friction on the piston and any misalignment of the pistons that might cause a bending moment (D. L. Kohlstedt, personal communication, 2014). This type of uncertainty is likely to result in interrun biases (Figure 1). Using the statistical model of equation (1), we can handle multiple experimental runs jointly in our MCMC sampling by estimating such biases together with flow law parameters.

can be determined by calculating the autocorrelation function. From a resampled ensemble, we can readily calculate the mean and covariance of model parameters. In order to verify the convergence of MCMC sampling, we need to run the sampling with multiple initial models and compare the results of these so-called parallel runs. If different runs result in nearly identical statistical distributions, we may conclude that the parameter space has been fully explored.

### 3. Deformation Data

The deformation data of BMK91 on single crystals of San Carlos olivine,  $(Mg_{0.91}Fe_{0.09}Ni_{0.003})_2SiO_4$ , were all collected in controlled chemical environments at a total pressure of 0.1 MPa. Strain rates were measured as a function of stress, temperature, and oxygen fugacity, and the effects of orthopyroxene activity and loading orientation were also investigated. Three loading orientations were tested:  $[110]_c$ ,  $[101]_c$ , and  $[011]_c$ , which favor slip on the  $(010)[100]$  system, duplex slip on the  $(001)[100]$  major system and  $(100)[001]$  minor system, and slip on the  $(010)[001]$  system, respectively. For each loading orientation, two different buffers are used to control the activity of orthopyroxene, one with orthopyroxene (opx) of composition  $Mg_{0.9}Fe_{0.1}SiO_3$  and the other with magnesiowustite (mw) of composition  $Mg_{0.7}Fe_{0.3}O$ . For further details on experimental conditions, see BMK91. All of original experimental data are reported in Bai [1990].

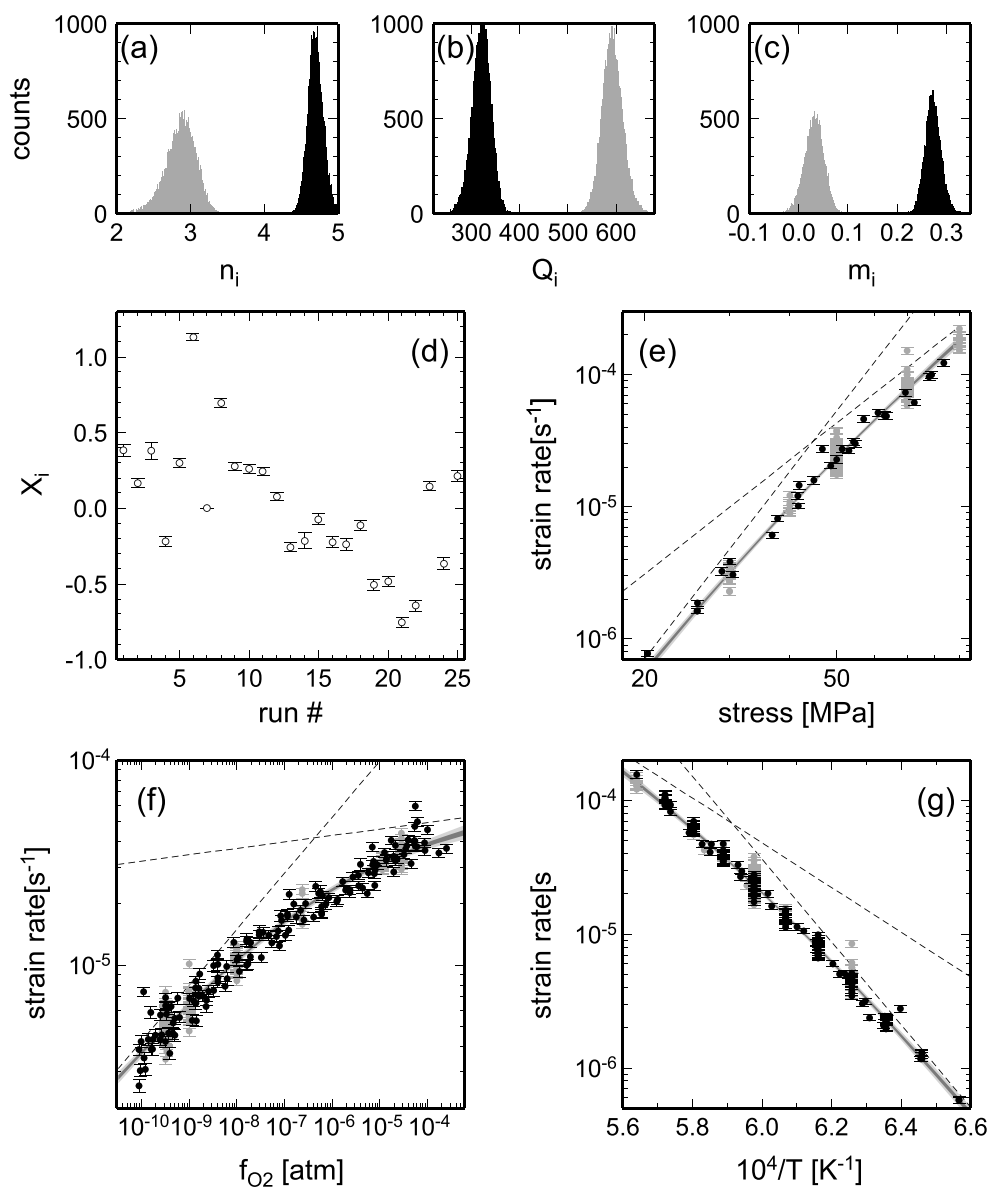


**Figure 6.** Results of joint inversion with all experimental runs for  $[101]_c$  with opx buffer. Distribution of (a) the stress exponents  $n_1$  (solid) and  $n_2$  (gray), (b) the activation enthalpies  $Q_1$  (solid) and  $Q_2$  (gray), and (c) the oxygen fugacity exponents  $m_1$  (solid) and  $m_2$  (gray). (d) Summary of inter-run bias factors. Comparison of experimental data (circles) with prediction based on estimated flow law parameters in (e) stress versus strain rate, (f) oxygen fugacity versus strain rate, and (g) inverse temperature versus strain rate. The following reference state,  $T = 1673$  K,  $\sigma = 50$  MPa, and  $f_{O_2} = 10^{-6}$  atm, is used to project experimental data into these covariation plots. Error bar includes all experimental uncertainties and bias correction is applied. Solid circles denote data from primary experimental runs, e.g., variable-stress runs in Figure 6e. Dashed lines denote the prediction of individual flow laws, and dark and light gray denote 50% and 90% confidence limits, respectively. Run numbers 1 to 25 refer to 7601a, 7601b, 7301a, 7301b, 7301c, 7301d, 5202, 5207, 5215, 6104, 6201, 6202, 6302a, 6302b, 6302c, 6401, 6403a, 6403b, 6503c, 6406a, 6406b, 6407, 7101, 7102, and 7103, respectively, and run 5202 is used as a reference for inter-run biases.

#### 4. Inversion With Individual Experimental Runs

In this section, we report results from our reanalysis of individual experimental runs. BMK91 analyzed each experimental run separately and then combined these individual results to derive their final estimates on flow law. As discussed later in section 6.1, this second step is problematic, but the first step by itself contains no major issue. Our reanalysis in this section corresponds exactly to the nonlinear regression conducted by

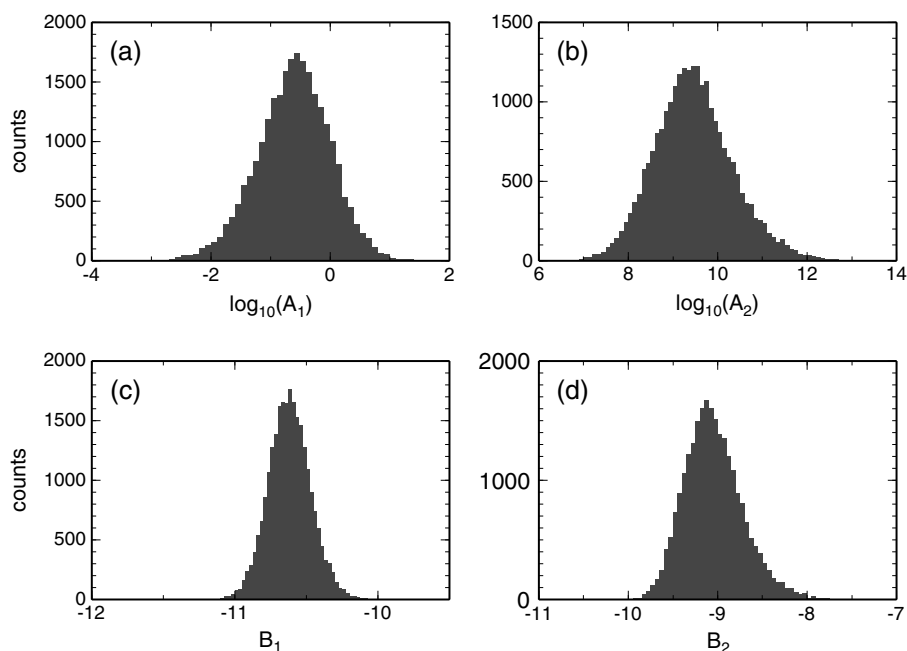


**Figure 7.** Distribution of scaling constants in their original form: (a)  $A_1$  and (b)  $A_2$ , and in the  $Q$ -normalized form: (c)  $B_1$  and (d)  $B_2$ , for the case of  $[101]_c$  with opx buffer.

BMK91, and as it is considerably simpler than inversions with combined data sets (section 5), it serves as a preparatory demonstration of the new MCMC algorithm.

The experimental runs of BMK91 consist of three types: (1) variable stress with constant temperature and oxygen fugacity, to determine the stress exponents  $n_i$ ; (2) variable oxygen fugacity with constant stress and temperature, to determine the oxygen fugacity components  $m_i$ ; and (3) variable temperature with constant stress and oxygen fugacity, to determine the activation enthalpy  $Q_i$ . Each run of the first type can be fit with a single stress exponent, but runs of other types require multiple exponents or activation enthalpies as mentioned in section 3. The a priori ranges are set as  $[1.0, 6.0]$  for the stress exponents,  $[-0.1, 1.0]$  for the oxygen fugacity exponents, and  $[0, 1500]$  (in  $\text{kJ mol}^{-1}$ ) for the activation enthalpies. These ranges are wide enough to encompass all inversion results of *Bai et al.* [1991]. When experimental runs are considered individually, there is no need to model interrune bias, so the bias parameter  $X$  is set to zero. The maximum number of MCMC iterations is  $10^5$ , with  $D = 10$ ,  $P = 75$ , and  $C = 10$ , and an ensemble was resampled with an interval of 100. So the size of a resampled ensemble is  $10^3$  for each run.

Examples of MCMC inversion results are shown in Figure 2. Predicted strain rates based on fitted model parameters are consistent with the measured strain rates. In many cases, the normalized (full) cost function,  $\chi_f^2/N$ , where  $N$  is the number of relevant data, is greater than unity (i.e., the misfit between data and model prediction exceeds data uncertainty on average), indicating that the prescribed experimental uncertainty is underestimated. This sort of observation, if available while conducting experiments, would be useful to reevaluate the variability of an experimental environment. Here we proceed with the aforementioned experimental uncertainty, as it is impractical to speculate on experiments conducted many years ago.

All of individual inversion results are summarized in Tables C1 to C3, along with the original results of BMK91. The original and new results are also compared in Figure 3. An excellent correspondence is observed for the stress exponents (Figure 3a), which may not be surprising because the relevant inversion involves only two model parameters,  $A$  and  $n$ . It may also be seen that the MCMC inversion results are generally characterized by smaller parameter uncertainty. Correspondences for the oxygen fugacities and activation enthalpies are similarly good for most cases. Cases with poor correspondence almost always involve a very large parameter error in the original estimate. In fact, for a number of fugacity exponents and activation enthalpies, BMK91 did not report parameter uncertainty or reported only upper or lower bound (see Tables C2 and C3). Given the benchmark tests of our MCMC code using synthetic data (Appendix B), we suspect that the regression algorithm adopted by BMK91 failed to deconvolve flow law parameters in some

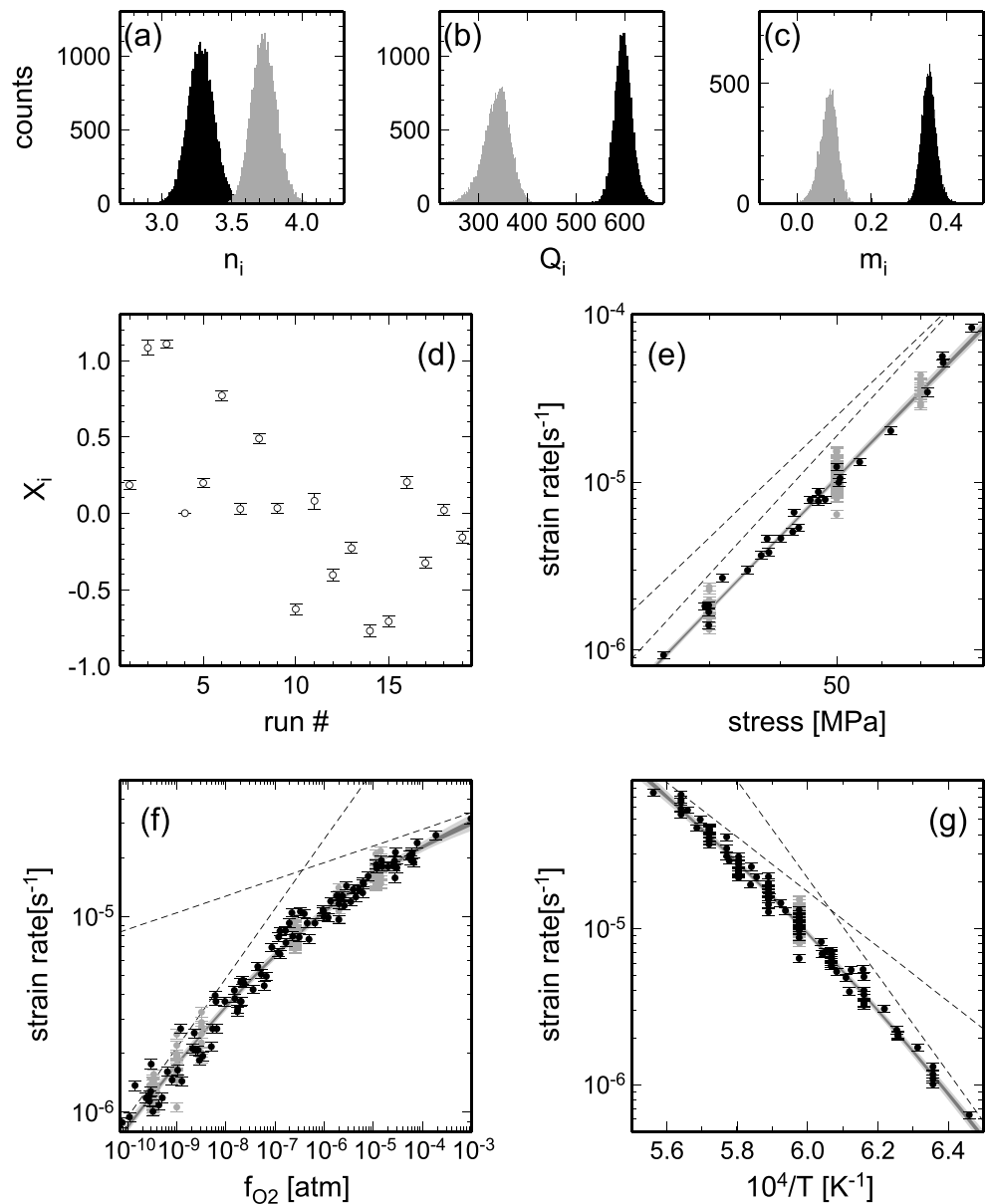


**Figure 8.** Same as Figure 6 but for the case of  $[101]_c$  with mw buffer. Run numbers 1–19 refer to W504a, 7602a, 7602b, W503, W504b, 5207, 5215, 6104, 6201, W503, 6402, 6404a, 6404b, 6405a, 6405b, 7104, 7105, 7106, and 7107, respectively. Run W503 is used as a reference.

cases. Nonetheless, it is safe to conclude that, at least for the inversion of individual runs, there is no major discrepancy between our results and the original results of BMK91.

### 5. Joint Inversion With Combined Data Sets

Inversion results in this section constitute the main results of this paper. Inversions in the previous section were conducted mostly to facilitate a comparison with BMK91, and what will be presented below is entirely independent from these earlier results. In this section, experimental runs with the same combination of buffer and orientation are combined to estimate all relevant flow law parameters simultaneously. For  $[101]_c$  with opx buffer, for example, there are 2 variable-stress runs, 10 variable-oxygen-fugacity runs, and 13 variable-temperature runs, and these 25 runs are considered jointly to determine a pair of scaling constants, stress exponents, oxygen fugacity exponents, and activation enthalpies, along with 24 interrun biases. Traditionally, stress exponents are determined from variable-stress experiments, but even experiments under

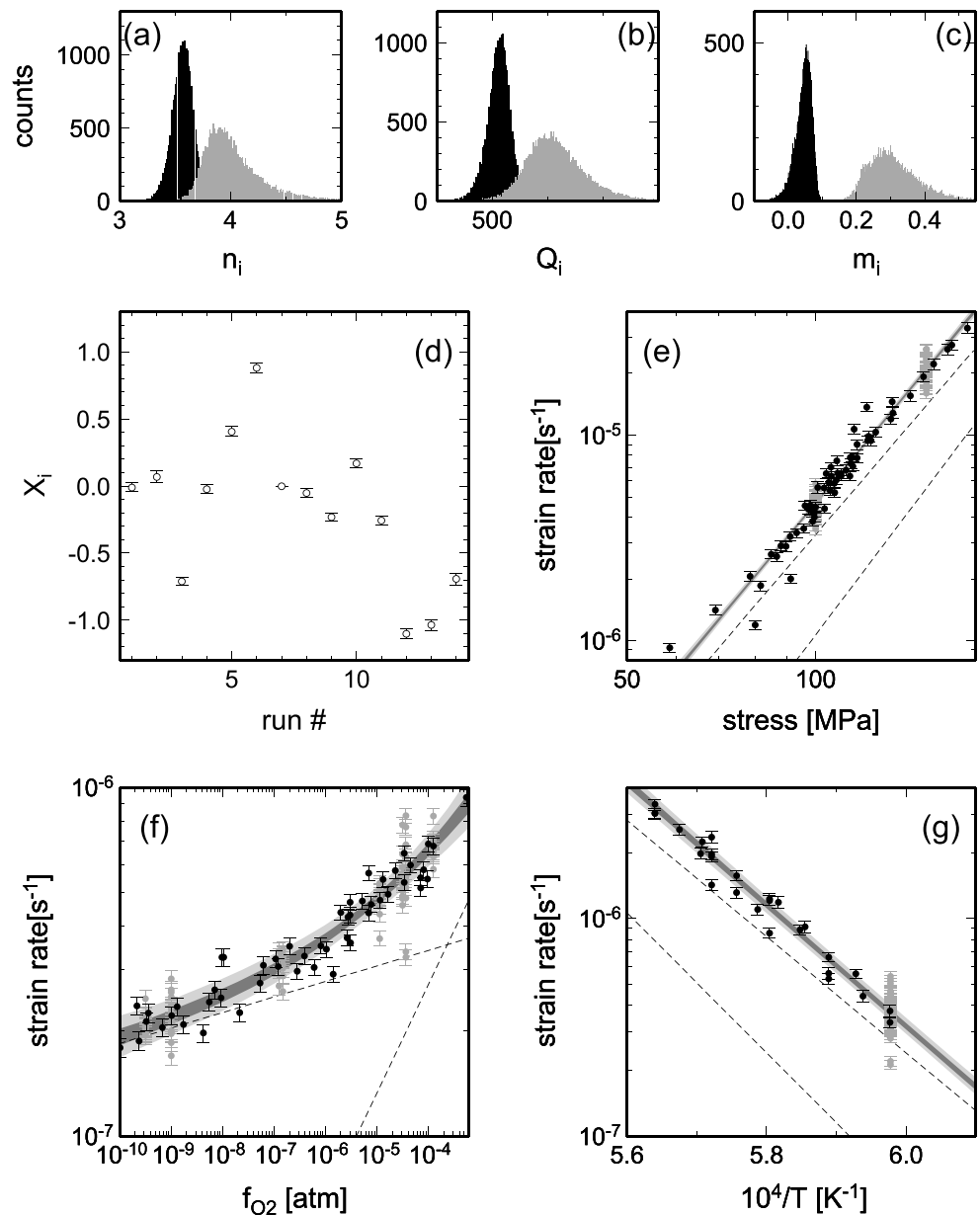


**Figure 9.** Same as Figure 6 but for the case of  $[011]_c$  with opx buffer. Run numbers 1–14 refer to 5105a, 5105b, 5109, 7503, 7504a, 7504b, 5101, 5212, 5214, 6101, 6203, 6601, 6602a, and 6602b, respectively. Run 5101 is used as a reference.

constant stress can contribute to the estimate of stress exponents, if interrun biases are taken into account properly. Similar statements can be made for other flow law parameters as well, and jointly inverting all relevant runs maximizes experimental constraints.

The a priori ranges for flow law parameters are the same as specified in the previous section, and that for the bias parameters  $X_m$  is set as  $[\log(10^{-0.5}), \log(10^{0.5})]$ . The maximum number of MCMC iterations is  $10^6$ , with  $D = 100$ ,  $P = 75$ , and  $C = 10$ . Based on the autocorrelation function of MCMC sequences (Figure 4), each ensemble was resampled with an interval of 200, except for  $[110]_c$  with opx buffer, for which a resampling interval of 500 was used. The case of  $[110]_c$  with opx buffer represents the most complex inversion in this paper with the largest number of model parameters, so it took more iterations to sufficiently perturb all parameters by random-scan Gibbs sampling. For each buffer-orientation pair, five parallel MCMC runs were conducted. For most combinations, these parallel runs yielded nearly identical results (Figure 5), so these

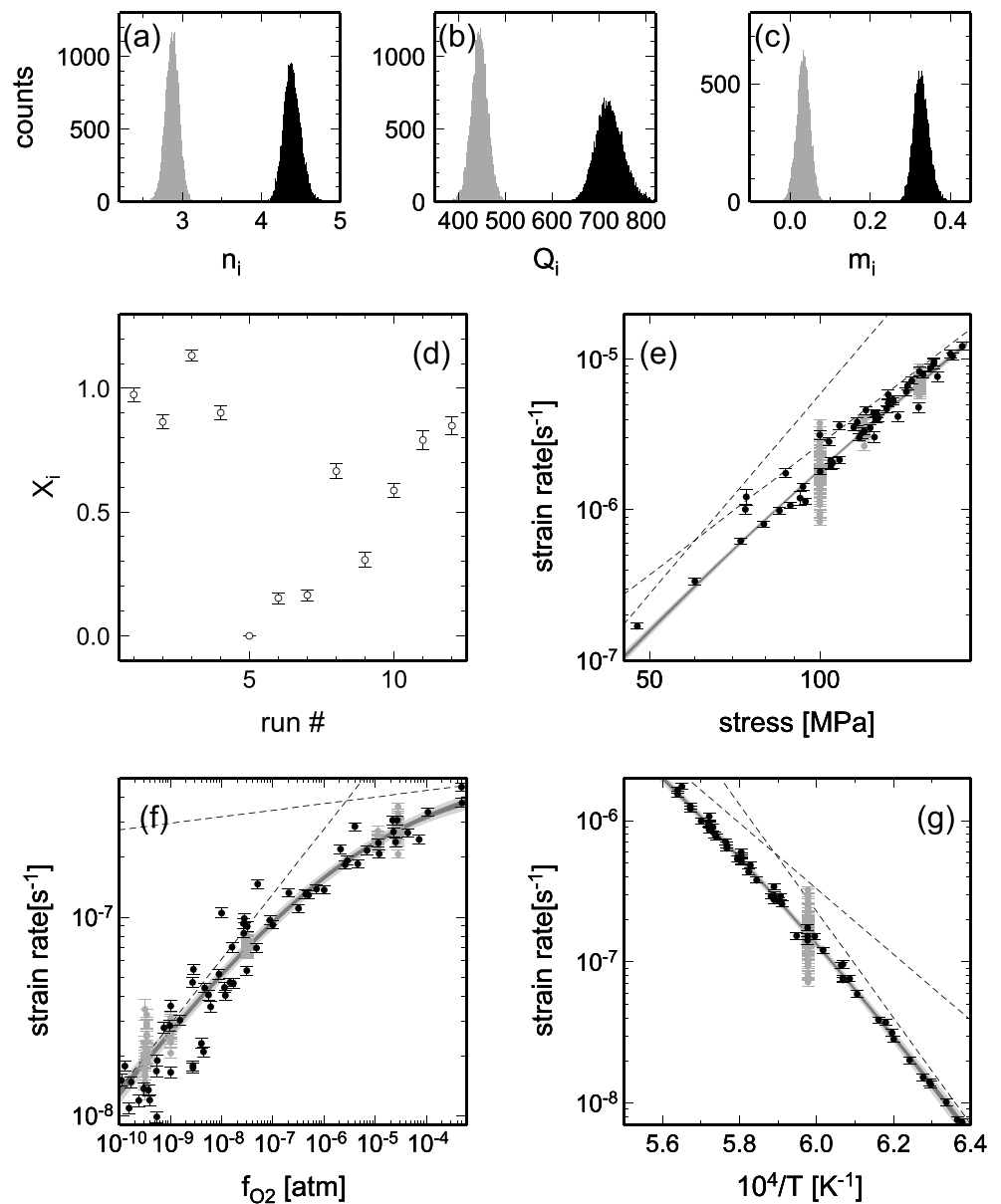


**Figure 10.** Same as Figure 6 but for the case of [011]<sub>c</sub> with mw buffer. Run numbers 1–12 refer to 7501a, 7501b, 7502a, 7502b, 5104, 5107, 5110, 6203, 6603a, 6603b, 7401, and 7402, respectively. Run 5104 is used as a reference.

runs were gathered to form an ensemble with  $2.5 \times 10^4$  samples for each pair. The case of [110]<sub>c</sub> with opx buffer is different and will be described later.

Results for the case of [101]<sub>c</sub> with opx buffer are summarized in Figure 6. All of six flow-law parameters are well resolved as  $n_1 = 4.70 \pm 0.11$ ,  $n_2 = 2.86 \pm 0.21$ ,  $m_1 = 0.27 \pm 0.02$ ,  $m_2 = 0.03 \pm 0.02$ ,  $Q_1 = 320 \pm 20$  kJ mol<sup>-1</sup>, and  $Q_2 = 593 \pm 22$  kJ mol<sup>-1</sup>. Most of bias parameters are found to be within  $\pm 0.5$  (Figure 6d), corresponding to interrun biases of  $\sim 10^{\pm 0.2}$ . This magnitude of bias is compatible to what is indicated in Figure 1. A comparison with single-run inversion results is informative. There are two variable-stress runs, which yielded two estimates on the stress exponent,  $3.39 \pm 0.05$  (at  $T = 1400^\circ\text{K}$  and  $f_{O_2}$  of  $3.2 \times 10^{-5}$  atm) and  $3.98 \pm 0.05$  (at  $T = 1400^\circ\text{C}$  and  $f_{O_2}$  of  $3.2 \times 10^{-10}$  atm) (Table C1). Given the operation of two sequential mechanisms, these values are best regarded as an effective exponent, being intermediate between the two actual exponents (Figure 6e). A joint inversion is thus essential to deconvolve multiple stress exponents, and it is also important for oxygen fugacity exponents and activation enthalpies. Though single-run inversions were able to deconvolve multiple  $m_i$ s and  $Q_i$ 's (Tables C2 and C3), estimated parameter values are all “apparent” values

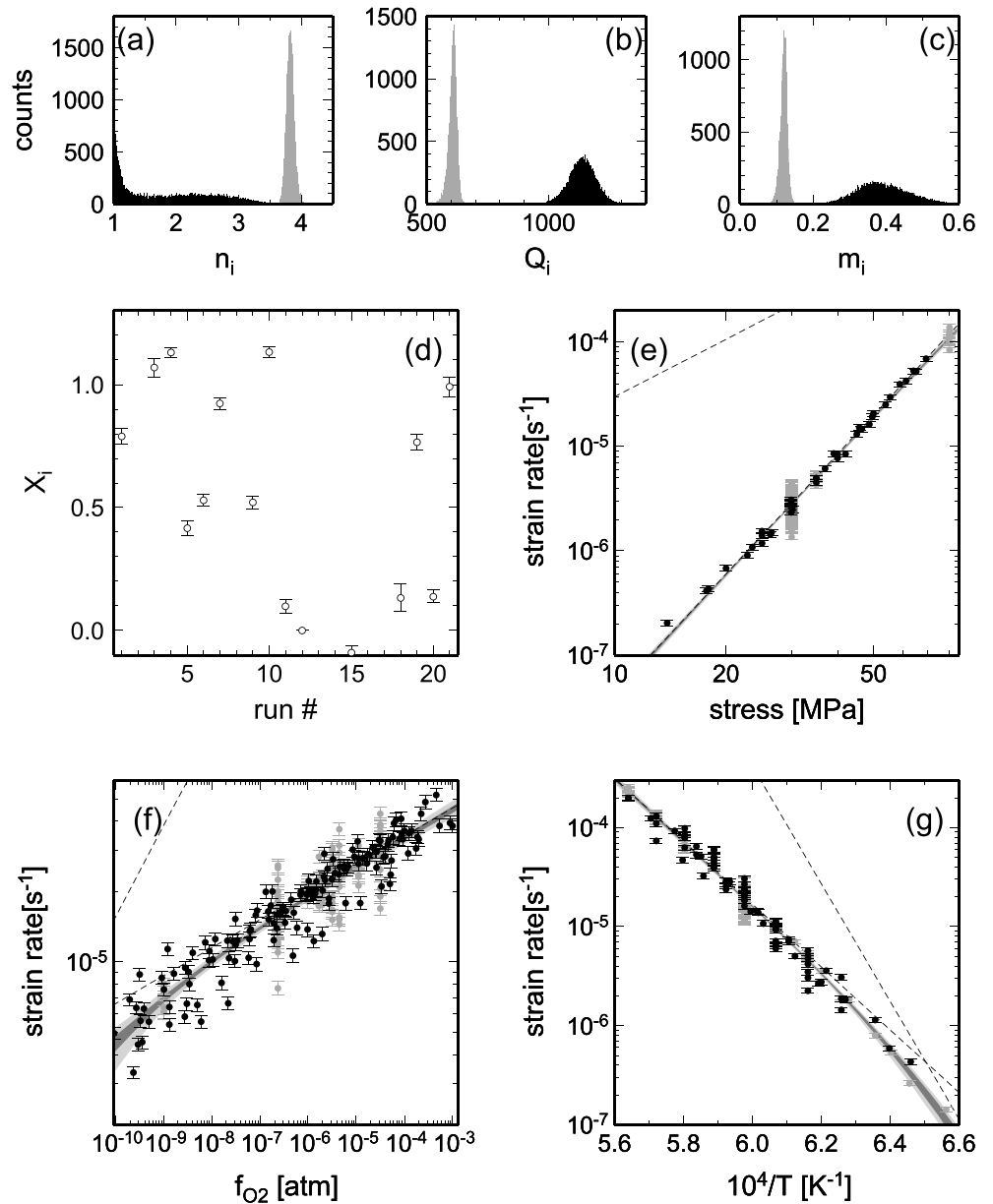


**Figure 11.** Same as Figure 6 but for the case of  $[110]_c$  with mw buffer. Run numbers 1–21 refer to S502, S504, 7703a, 7703b, S501a, S501b, 5201, 5210, 5213c, 6103, 6204a, W504, 7202a, 7206, S501, 6204b, 6204c, 6501a, 6501b, 7202b, and 7206, respectively. Run W504 is used as a reference.

at constant temperature and stress (for  $m_i$ ) or at constant  $f_{O_2}$  and stress (for  $Q_i$ ). One cannot arrive at the  $m_i$ s and  $Q_i$ s used in equation (4) by simply averaging these apparent values. Figure 7 compares the distributions of  $\log_{10} A_i$  with those of  $B_i$ , with the latter defined as

$$B_i = \log_{10} \left( A_i \exp \left( \frac{-Q_i}{RT_{ref}} \right) \right), \quad (10)$$

where  $T_{ref}$  is set to 1673 K. Small changes in  $Q_i$  can induce very large variations in  $A_i$ , so the use of  $B_i$  instead of  $A_i$  results in more compact distributions, which help the statistical characterization of an MCMC ensemble.

Results for other buffer-orientation pairs are similarly summarized in Figures 8–12 and Table 2. As in the case of  $[101]_c$  with opx buffer, all flow law parameters are well resolved in the cases of  $[101]_c$  and  $[011]_c$  with mw buffer (Figures 8 and 10). In the case of  $[011]_c$  with opx buffer, one of two parallel mechanisms is characterized by greater uncertainty (Figure 9), and in the case of  $[110]_c$  with mw buffer, one of two

**Table 2.** Joint Inversion Results

Parameter	<i>Bai et al.</i> [1991]	This Study
<i>[101]<sub>c</sub> opx Buffer</i>		
$\dot{\epsilon} = [(\dot{\epsilon}_1)^{-1} + (\dot{\epsilon}_2)^{-1}]^{-1}$		
$n_1$	$3.5 \pm 0.1$	$4.70 \pm 0.11$
$Q_1$	$250 \pm 50$	$320 \pm 20$
$m_1$	$0.33 \pm 0.05$	$0.27 \pm 0.02$
$A_1$	$0.65^{+0.06}_{-0.06}$	$0.23^{+0.1}_{-0.07}$
$B_1$	-	$-1.06 \pm 0.15$
$n_2$	$3.5 \pm 0.1$	$2.86 \pm 0.21$
$Q_2$	$690 \pm 130$	$593 \pm 22$
$m_2$	$0.06 \pm 0.02$	$0.03 \pm 0.02$
$A_2$	$5.3^{+0.6}_{-0.6} \times 10^{11}$	$2.93^{+3.35}_{-1.56} \times 10^9$
$B_2$	-	$-9.04 \pm 0.33$
<i>[101]<sub>c</sub> mw Buffer</i>		
$\dot{\epsilon} = [(\dot{\epsilon}_1)^{-1} + (\dot{\epsilon}_2)^{-1}]^{-1}$		
$n_1$	$3.5 \pm 0.1$	$3.28 \pm 0.09$
$Q_1$	$700 \pm 170$	$597 \pm 18$
$m_1$	$0.40 \pm 0.05$	$0.35 \pm 0.02$
$A_1$	$1.0^{+0.1}_{-0.1}$	$40^{+35}_{-19}$
$B_1$	-	$-8.04 \pm 0.27$
$n_2$	$3.5 \pm 0.1$	$3.73 \pm 0.09$
$Q_2$	$300 \pm 90$	$336 \pm 28$
$m_2$	$0.06 \pm 0.09$	$0.09 \pm 0.02$
$A_2$	$0.16^{+0.07}_{-0.05} \times 10^{11}$	$0.88^{+0.43}_{-0.29} \times 10^9$
$B_2$	-	$-1.06 \pm 0.17$
<i>[011]<sub>c</sub> opx Buffer</i>		
$\dot{\epsilon} = \dot{\epsilon}_1 + \dot{\epsilon}_2$		
$n_1$	$3.5 \pm 0.1$	$3.56 \pm 0.1$
$Q_1$	$540 \pm 50$	$511 \pm 22$
$m_1$	$0.02 \pm 0.02$	$0.04 \pm 0.03$
$A_1$	$2.1^{+0.3}_{-0.3} \times 10^4$	$4.0^{+3.7}_{-1.9} \times 10^3$
$B_1$	-	$-1.23 \pm 0.29$
$n_2$	$3.5 \pm 0.1$	$4.03 \pm 0.30$
$Q_2$	$540 \pm 50$	$615 \pm 62$
$m_2$	$0.23 \pm 0.05$	$0.31 \pm 0.08$
$A_2$	$5.2^{+0.6}_{-0.4} \times 10^5$	$1.1^{+3.0}_{-0.8} \times 10^7$
$B_2$	-	$-1.22 \pm 0.58$
<i>[011]<sub>c</sub> mw Buffer</i>		
$\dot{\epsilon} = [(\dot{\epsilon}_1)^{-1} + (\dot{\epsilon}_2)^{-1}]^{-1}$		
$n_1$	$3.5 \pm 0.1$	$4.39 \pm 0.11$
$Q_1$	$750 \pm 170$	$723 \pm 30$
$m_1$	$0.40 \pm 0.07$	$0.33 \pm 0.02$
$A_1$	$1.0^{+0.3}_{-0.2} \times 10^{14}$	$3.3^{+1.6}_{-1.1} \times 10^{10}$
$B_1$	-	$-1.21 \pm 0.17$
$n_2$	$3.5 \pm 0.1$	$2.87 \pm 0.09$
$Q_2$	$370 \pm 90$	$446 \pm 18$
$m_2$	$0.0 \pm 0.1$	$0.03 \pm 0.02$
$A_2$	$0.2^{+0.3}_{-0.1}$	$6.4^{+2.9}_{-2.0} \times 10^2$

**Table 2.** (continued)

Parameter	<i>Bai et al.</i> [1991]	This Study
$B_2$	-	$-1.11 \pm 0.16$
<i>[110]<sub>c</sub> opx Buffer</i>		
$\dot{\epsilon} = \dot{\epsilon}_1 + [(\dot{\epsilon}_2)^{-1} + (\dot{\epsilon}_3)^{-1}]^{-1}$		
$n_1$	$3.5 \pm 0.1$	$3.86 \pm 0.21$
$Q_1$	$230 \pm 60$	$320 \pm 60$
$m_1$	$0.36 \pm 0.05$	$0.25 \pm 0.02$
$A_1$	$0.02^{+0.01}_{-0.01}$	$0.86^{+1.2}_{-0.5}$
$B_1$	-	$-10.1 \pm 0.38$
$n_2$	$3.5 \pm 0.1$	$3.67 \pm 0.55$
$Q_2$	$1000 \pm 230$	$1170 \pm 190$
$m_2$	$0.10 \pm 0.07$	$0.16 \pm 0.04$
$A_2$	$1.3^{+6.6}_{-1.1} \times 10^{22}$	$3.5^{+19}_{-3} \times 10^{27}$
$B_2$	-	$-9.01 \pm 0.81$
$n_3$	$3.5 \pm 0.1$	$2.79 \pm 0.33$
$Q_3$	$290 \pm 70$	$414 \pm 82$
$m_3$	$0.15 \pm 0.1$	$0.09 \pm 0.03$
$A_3$	$1.2^{+0.3}_{-0.2}$	$1.6^{+2.9}_{-1.0} \times 10^4$
$B_3$	-	$-8.72 \pm 0.45$
<i>[110]<sub>c</sub> mw Buffer</i>		
$\dot{\epsilon} = [(\dot{\epsilon}_1)^{-1} + (\dot{\epsilon}_2)^{-1}]^{-1}$		
$n_1$	$3.5 \pm 0.1$	$1.83 \pm 0.7$
$Q_1$	$1000 \pm 200$	$1140 \pm 63$
$m_1$	$0.2 \pm 0.1$	$0.39 \pm 0.08$
$A_1$	$1.0^{+2.2}_{-0.7} \times 10^{22}$	$3.3^{+185}_{-3.2} \times 10^{31}$
$B_1$	-	$-4.0 \pm 1.76$
$n_2$	$3.5 \pm 0.1$	$3.82 \pm 0.12$
$Q_2$	$330 \pm 130$	$608 \pm 28$
$m_2$	$0.2 \pm 0.1$	$0.12 \pm 0.01$
$A_2$	$25^{+200}_{-20}$	$3.2^{+2.6}_{-1.4} \times 10^8$
$B_2$	-	$-1.05 \pm 0.26$

sequential mechanisms is barely resolved (Figure 11); most of relevant experimental data seem to require just one deformation mechanism.

The case of  $[110]_c$  with opx buffer deserves special attention because five parallel MCMC runs resulted in two sets of solutions (Figure 13). What is shown in Figure 12 is based on the combination of the second and third parallel runs; the other subset, composed of the first, fourth, and fifth runs, is characterized by more pathological statistical distributions (Figure D1), so it is not adopted as valid estimates. It is noted that these two subsets of MCMC solutions can explain the given data equally well, so we cannot discriminate between them purely on the basis of data fit. What is surprising is that each MCMC sequence in this particular case was able to sample only one of the two subsets; this behavior does not conform to our expectation for MCMC sampling. This may be caused by the hybrid nature of our sampling algorithm, which contains conjugate gradient search for scaling constants. The case of  $[110]_c$  with opx buffer thus underscores the importance of checking convergence with parallel runs.

## 6. Discussion

### 6.1. Comparison With *Bai et al.* [1991]

Our joint inversion results are listed in Table 2 with the flow law parameter estimates of BMK91. Whereas these two estimates are broadly consistent, they still differ in important ways. In this section, we discuss the causes of these differences.

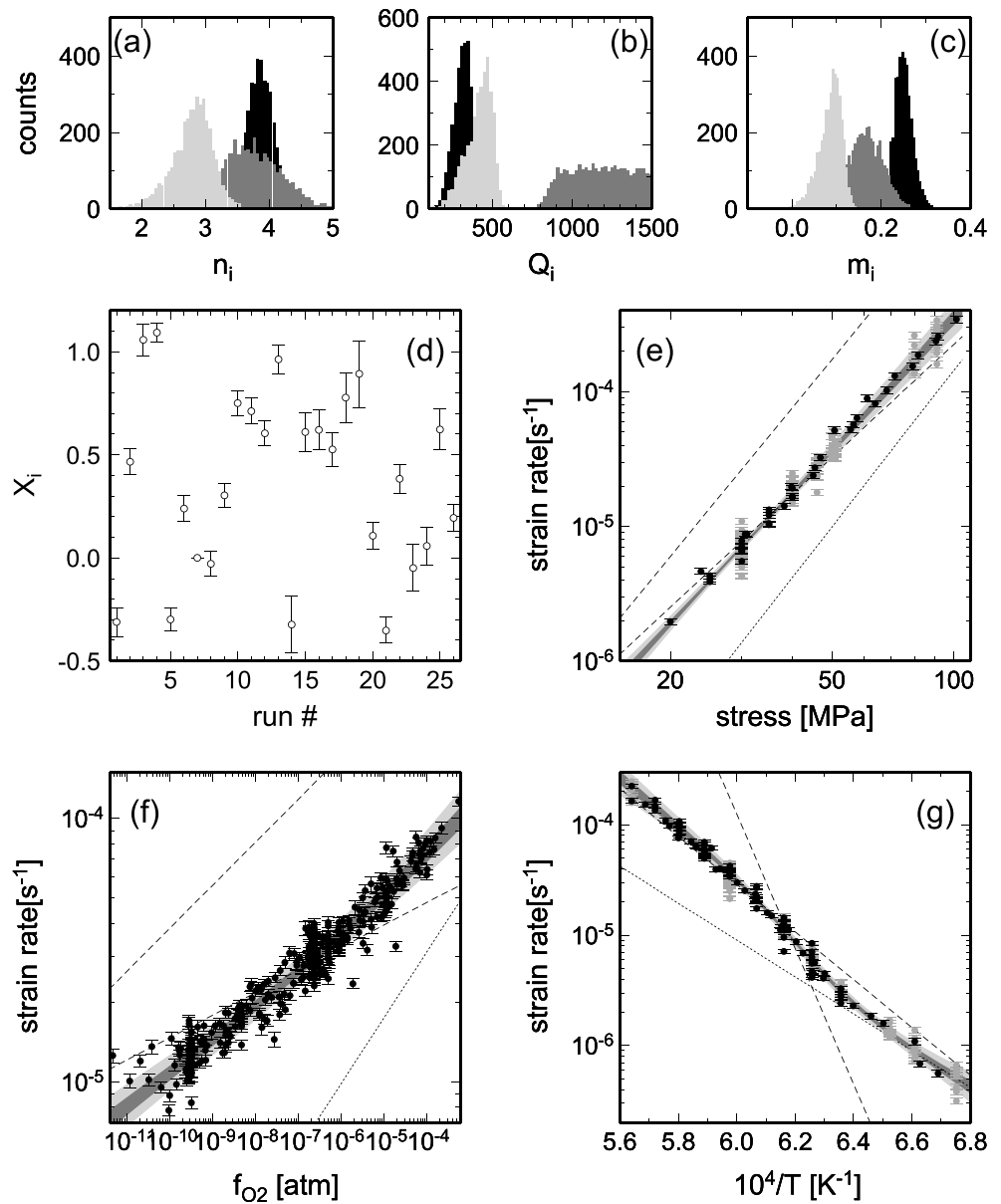


**Figure 12.** Same as Figure 6 but for the case of  $[110]_c$  with opx buffer. Results are based on the combination of parallel run numbers 2 and 3 (Figure 13). (a–c) Gray scale for histograms is the following: solid, medium gray, and light gray are, respectively, for parameters with subscript 1, 2, and 3. Run numbers 1–26 refer to S501, W501a, 7702a, 7702b, S501, S502, W501b, 5206, 5210, 5123a, 5213c, 6103, 6204, 7203a, 7204a, 7204b, 7205, 7701a, 7701b, S502, 6301, 7201, 7203b, 7203c, 7204, and 7205, respectively. Run W501b is used as a reference.

It should be made clear at the outset that, even though we list the estimates of BMK91 in the table for joint inversion results, their results are not based on joint inversion; they constructed these estimates by averaging the results of single-run inversions. For example, the activation enthalpy  $Q_1$  for  $[101]_c$  with opx buffer is estimated as  $250 \pm 50 \text{ kJ mol}^{-1}$  by averaging the results of three experimental runs:  $212 \pm 100 \text{ kJ mol}^{-1}$  (run 6302),  $260 \pm 90 \text{ kJ mol}^{-1}$  (run 6401), and  $270 \pm 90 \text{ kJ mol}^{-1}$  (run 7101). The averaging was done with the following weighted average formula:

$$\langle x \rangle = \frac{\sum_{i=1}^M w_i x_i}{\sum_{i=1}^M w_i}, \quad (11)$$

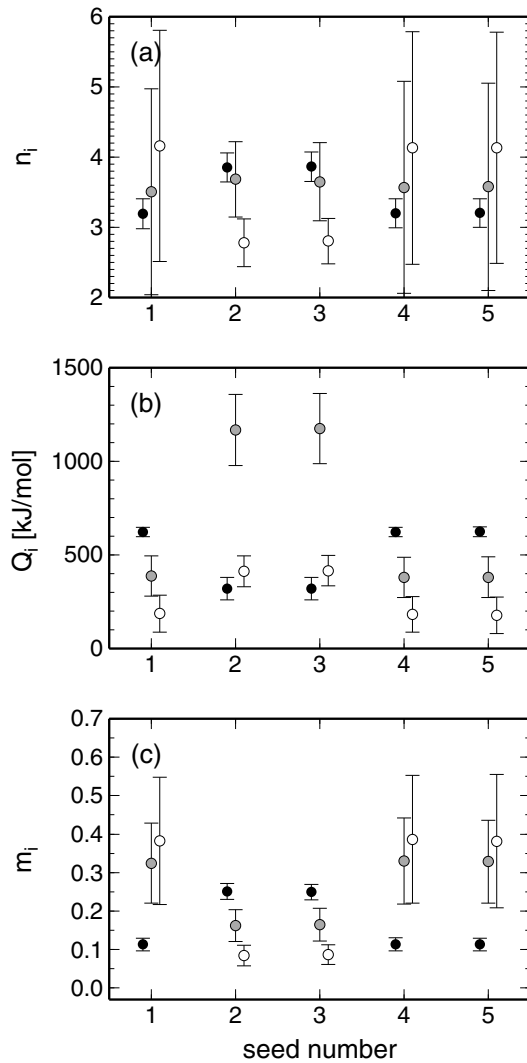


**Figure 13.** Comparison of results from five parallel MCMC runs for the case of  $[110]_c$  with opx buffer, in terms of mean and standard deviation: (a) the stress exponents  $n_1$  (solid),  $n_2$  (gray), and  $n_3$  (open), (b) the activation enthalpies  $Q_1$  (solid),  $Q_2$  (gray), and  $Q_3$  (open), and (c) the oxygen fugacity exponents  $m_1$  (solid),  $m_2$  (gray), and  $m_3$  (open).

where the weight  $w_i$  is calculated as  $\text{var}(x_i)^{-1}$  and  $\text{var}(x_i)$  is the variance of  $x_i$ . The variance of the average is given by

$$\text{var}(\langle x \rangle) = \left( \sum_{i=1}^M w_i \right)^{-1}, \quad (12)$$

and its square root gives the standard deviation.

There are three problems with their approach. First, many experimental runs were left unused. The case of  $[101]_c$  with opx buffer has a total of 13 variable-temperature runs, but as shown above, only 3 runs are used because the other 10 runs yielded only upper or lower bounds on  $Q_i$  (Table C3). Note that, with our MCMC inversion, these 10 runs do yield usable estimates; these runs contain valuable constraints on activation enthalpies. Second, as already mentioned in section 5, these single-inversion results are best regarded as apparent values, each being deconvolved with other state variables held constant (e.g., constant stress and oxygen fugacity in case of  $Q_i$ ), and variabilities seen in these results indicate that deconvolution was incomplete in each single-run inversion. Averaging such incomplete estimates does not necessarily lead to a more reliable estimate. Finally, BMK91 combined the results of all variable-stress runs from different buffer-orientation pairs and obtained a single estimate for the stress exponent as  $n = 3.5 \pm 0.1$ .

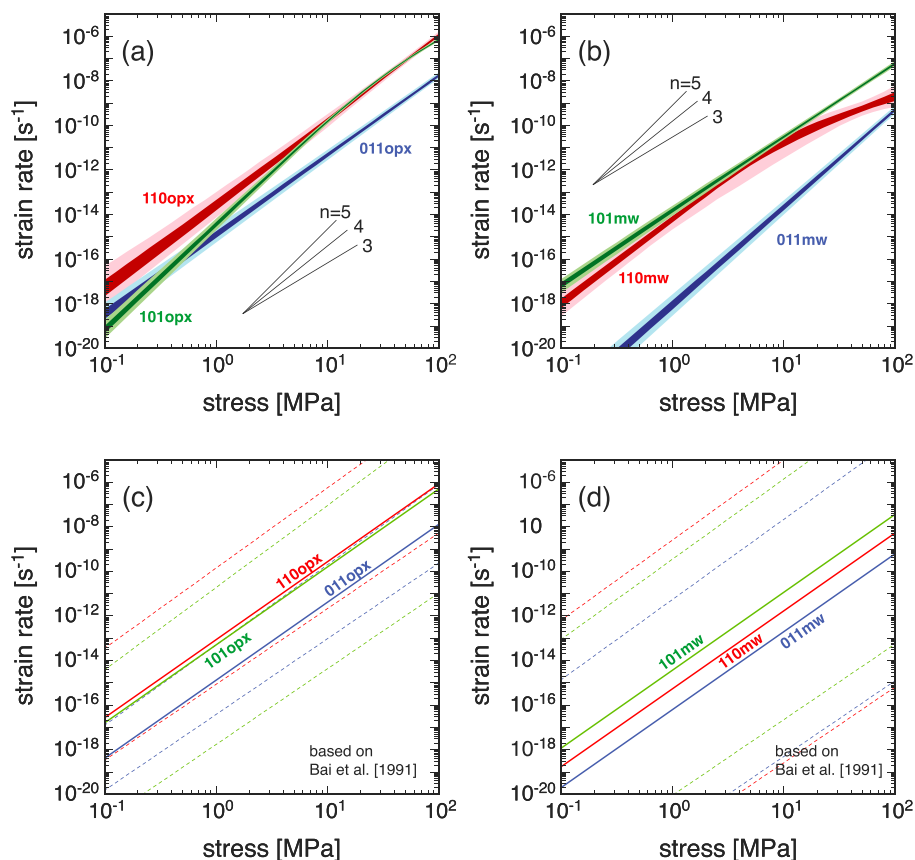


**Figure 14.** Prediction based on estimated flow law parameters in strain rate versus stress, at  $T=1473$  K and  $f_{O_2}=10^{-9}$  atm. Prediction based on the joint inversions of this study is shown in (a) for opx buffer and (b) for mw buffer. The cases of  $[110]_c$ ,  $[101]_c$ , and  $[011]_c$  are shown in red, green, and blue, respectively, and dark and light shadings denote 50% and 90% confidence limits, respectively. (c, d) Prediction based on the flow laws of BMK91 is shown. Dashed lines indicate the upper and lower bounds based on their estimate of parameter uncertainties. See text for details.

They then used this value for all stress exponents  $n_i$ , appearing in six different buffer-orientation pairs. This is problematic because equations (11) and (12) are valid only when samples are derived from the same distribution [e.g., Sivia, 2006]. As can be seen from their Table 2 or our Table C1, the stress exponents from single-run inversions are spread from  $\sim 3.0$  to  $\sim 5.0$  (see also Figure 3a), and most of these exponents are incompatible with such a tight estimate as  $3.5 \pm 0.1$ .

It had been computationally intractable to do a proper statistical analysis until recently, owing to the lack of an intermediate recourse between single-run inversion and joint inversion. To maximize the deconvolution of flow law parameters, it is necessary to use all available experimental constraints simultaneously, which in turn requires to estimate interrun biases, resulting in a fairly large number of model parameters ( $\sim 30$ ). Given the highly nonlinear nature of the cost function to be minimized, it is best to use importance sampling such as MCMC, which is still time-consuming. Among six buffer-orientation pairs considered in this study, MCMC runs for the case of  $[011]_c$  with opx buffer were the fastest, each completed within 2 weeks (on Mac Pro with 3.06 Hz six-core Intel Xeon), and those for  $[110]_c$  with opx buffer were the slowest, taking about 6 weeks. Conducting deformation experiments, however, usually takes much longer, so spending a few extra weeks on data analysis may not be so demanding if we want to maximize the scientific benefits of an experimental study.

## 6.2. Implications for Fabric Transitions

The relative strength of various slip systems in a crystal controls the deformation fabrics (lattice-preferred orientation) of a polycrystalline aggregate [e.g., Karato, 2008, chap. 14]. The relative strength of slip systems could change with several parameters including the stress, water content, and pressure. In a classic work by Carter and Ave Lallemand [1970], they reported a few fabric transitions in the temperature-strain rate space.

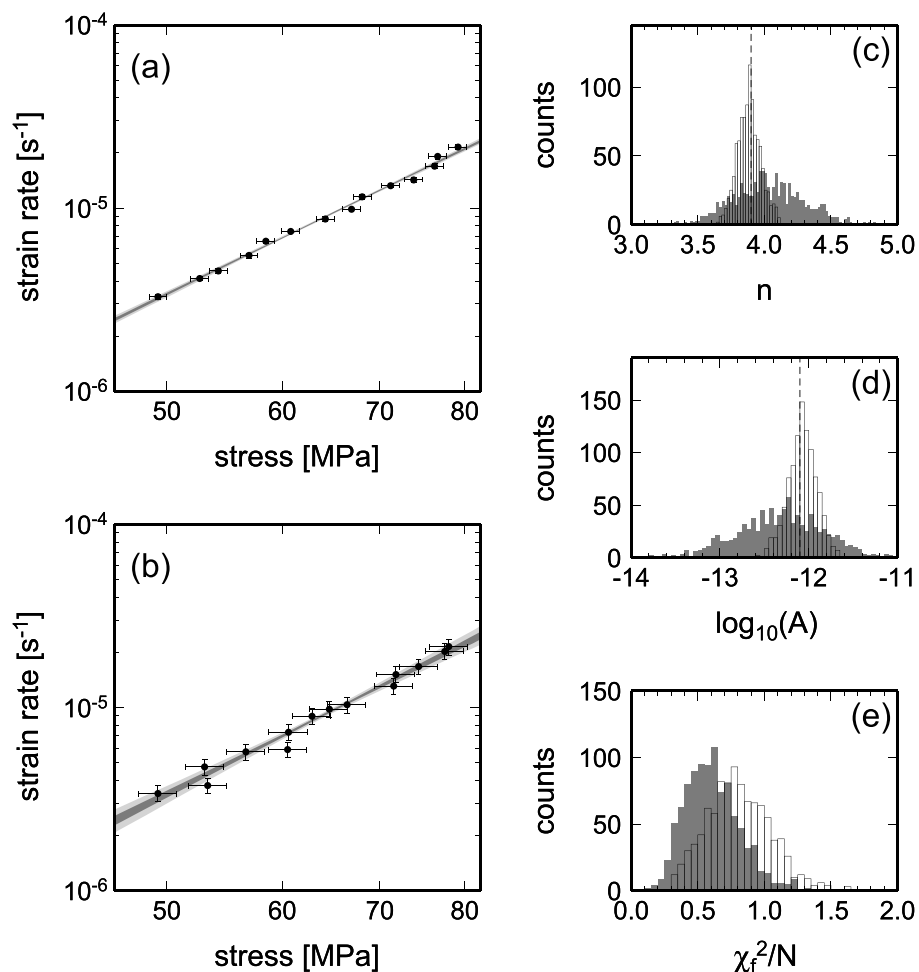


**Figure B1.** Results of benchmark tests with variable-stress data. Data and flow law prediction are shown in (a) for the first data set and in (b) for the second data set. Dark and light shadings denote 50% and 90% confidence limits, respectively. Also shown are the distributions of (c) the stress exponent, (d) scaling constant, and (e) normalized  $\chi_f^2$ . Open and filled histograms correspond to inversion with the first and second data sets, respectively. In Figures B1c and B1d, dashed lines indicate the location of true values.

These fabric transitions can, however, be interpreted as stress-induced fabric transitions [Karato *et al.*, 2008]. Karato *et al.* [2008] discussed that this observation is inconsistent with the results by Bai *et al.* [1991], where they reported that the stress exponent is common to all the slip systems ( $n = 3.5$ ). Karato *et al.* [2008] proposed that this apparent discrepancy might be due to the contribution of the Peierls mechanism, which would provide higher stress sensitivity for a slip system with a high Peierls barrier, i.e., a slip system with a longer Burgers vector ( $\mathbf{b} = [001]$  slip systems in olivine). Our present analysis provides the results that are largely consistent with this view, in the sense that the stress exponent tends to be higher for  $\mathbf{b} = [001]$  slip systems than for the  $\mathbf{b} = [100]$  slip systems. However, the influence of oxygen fugacity and oxide buffer complicates the issue.

### 6.3. Importance of Covariance

Table 2 reports the results of joint inversion in terms of mean and standard deviation. The uncertainty of an estimated flow law is usually reported in this manner, but this information alone is not sufficient. As an example, consider again the case of  $[101]_c$  with opx buffer, which has eight flow law parameters in total,  $n_1, n_2, m_1, m_2, Q_1, Q_2, A_1,$  and  $A_2$  (or  $B_i$  instead of  $A_i$ ). When we want to conduct a sensitivity test by perturbing these parameters within their uncertainties, how should we proceed? For example,  $Q_1$  is estimated as  $320 \pm 20 \text{ kJ mol}^{-1}$ . To see the effect of higher activation enthalpy, can we raise it to  $340 \text{ kJ mol}^{-1}$ , with all other parameters fixed? The answer is no, because the uncertainty of  $Q_1$  is correlated with the uncertainties

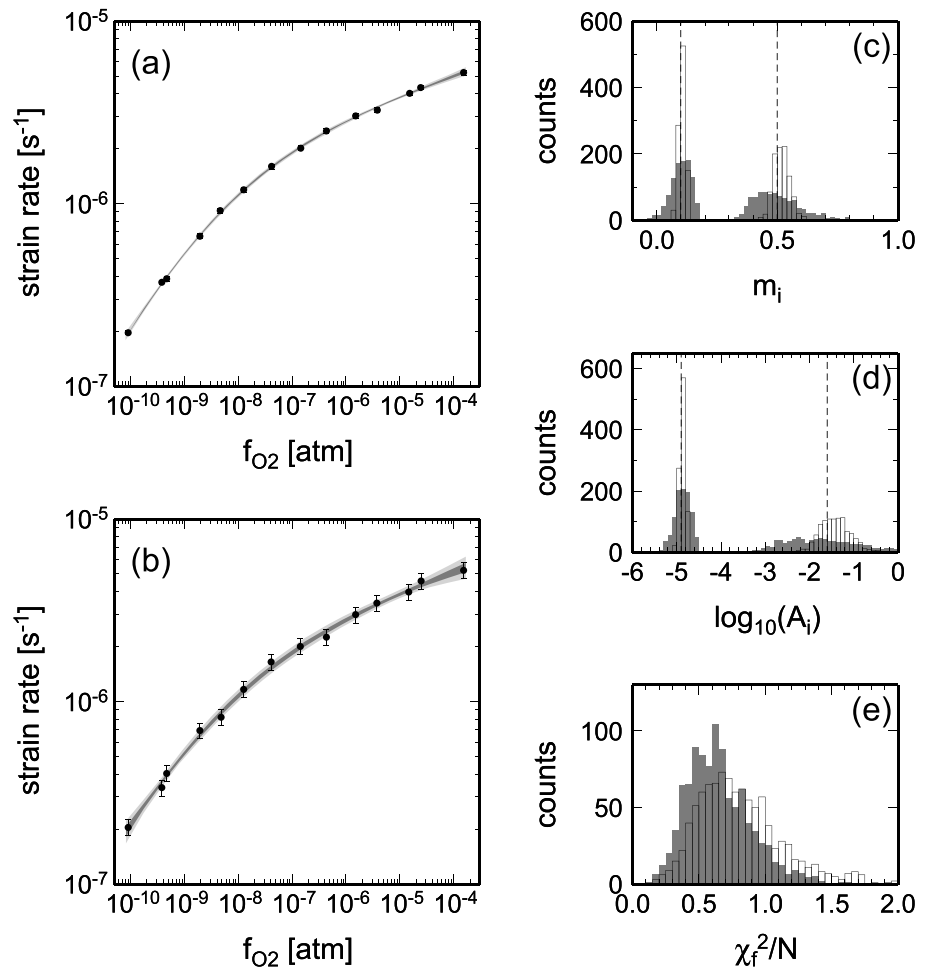


**Figure B2.** Similar to Figure B1 but for benchmark tests with variable  $f_{O_2}$  data generated from two sequential deformation mechanisms.

of other parameters. Other parameters have to be perturbed as well, not randomly to each other, but in accordance with the correlation exhibited by the MCMC ensemble.

Parameter correlation may be reported in the form of a correlation coefficient matrix, which is a normalized version of a covariance matrix, i.e.,

$$\rho(q_i, q_j) = \frac{\text{cov}(q_i, q_j)}{(\text{var}(q_i)\text{var}(q_j))^{1/2}}, \quad (13)$$

where  $\text{cov}(q_i, q_j)$  denotes the covariance between flow law parameters  $q_i$  and  $q_j$ , and  $\text{var}(q_i)$  denotes the variance of  $q_i$ . The correlation coefficient matrices based on the MCMC ensembles are given in Table D1 for all buffer-orientation pairs. The use of  $B_i$  instead of  $A_i$  is important here to extract correlation between scaling constants and other flow law parameters in a more meaningful manner. It may be observed that, in case of  $[101]_c$  with opx buffer,  $Q_1$  is negatively correlated with  $n_1, n_2, m_1, m_2$ , and  $B_1$ , and positively correlated with  $Q_2$  and  $B_2$ . When  $Q_1$  is perturbed to a higher value, therefore, the parameters in the first group should be perturbed downward, and those in the second group upward. In general, one can generate an ensemble of perturbed flow laws consistent with a given correlation coefficient matrix in the following way. First, construct a correlated, normally distributed random number matrix  $P$  of size  $J \times K$ , where  $J$  is the desired size of the ensemble, using the Cholesky decomposition of the correlation coefficient matrix [e.g., Rubinstein, 1981, §3.5.3]. Then, perturb model parameters using  $P$  as

$$q_k^j = \langle q_k \rangle + \text{var}(q_k)^{1/2} P_{jk}, \quad (14)$$

where  $k$  runs from 1 to  $K$  and  $j$  from 1 to  $J$ .

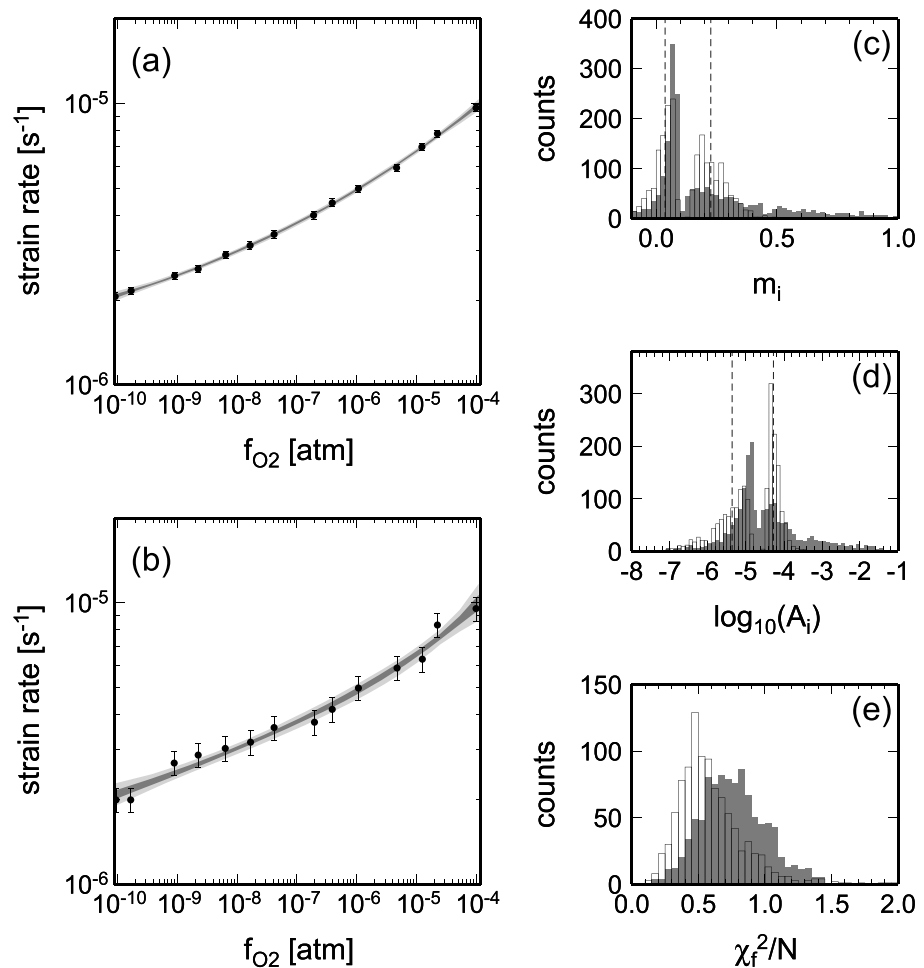


**Figure B3.** Similar to Figure B1 but for benchmark tests with variable  $f_{O_2}$  data generated from two parallel deformation mechanisms.

As a worked example, we generated a perturbed flow law ensemble with  $J = 10^3$  for each buffer-orientation pair and used it to evaluate the uncertainty associated with extrapolation to geological stress levels (Figures 14a and 14b). Here the temperature is fixed at 1473 K, and the oxygen fugacity is set to  $10^{-9}$  atm (approximately corresponding to the FMQ buffer). The hardest or easiest orientation of deformation could vary with stress. For opx buffer, the hardest orientation is  $[011]_c$  under laboratory conditions (10–100 MPa), but it becomes  $[101]_c$  under lithospheric conditions ( $10^{-1}$ – $10^{-2}$  MPa [Chu and Korenaga, 2012]). Extrapolation for  $[110]_c$  suffers from greatest uncertainty. It is interesting to see that, for opx buffer, strain rates for all three orientations become similar at geological stress levels, facilitating to satisfy the von Mises criterion [Karato, 2008]. In contrast, for mw buffer,  $[011]_c$  remains considerably more difficult to deform than other two orientations.

A similar exercise cannot be done with the flow laws of BMK91, because parameter covariance is not available; it is impossible to calculate covariance with their weighted average approach. Covariance between two parameters emerges only when these parameters are simultaneously estimated. One end-member exercise we may try with the reported uncertainties is to calculate the upper and lower bounds, assuming that all uncertainties are uncorrelated. The upper bound, for example, may be calculated by raising the scaling constants and the exponents for stress and oxygen fugacity and lowering the activation enthalpies. As seen in Figures 14c and 14d, such bounds are clearly incompatible with experimental data. The importance of calculating covariance, which in turn requires conducting joint inversions, may be evident in this example.

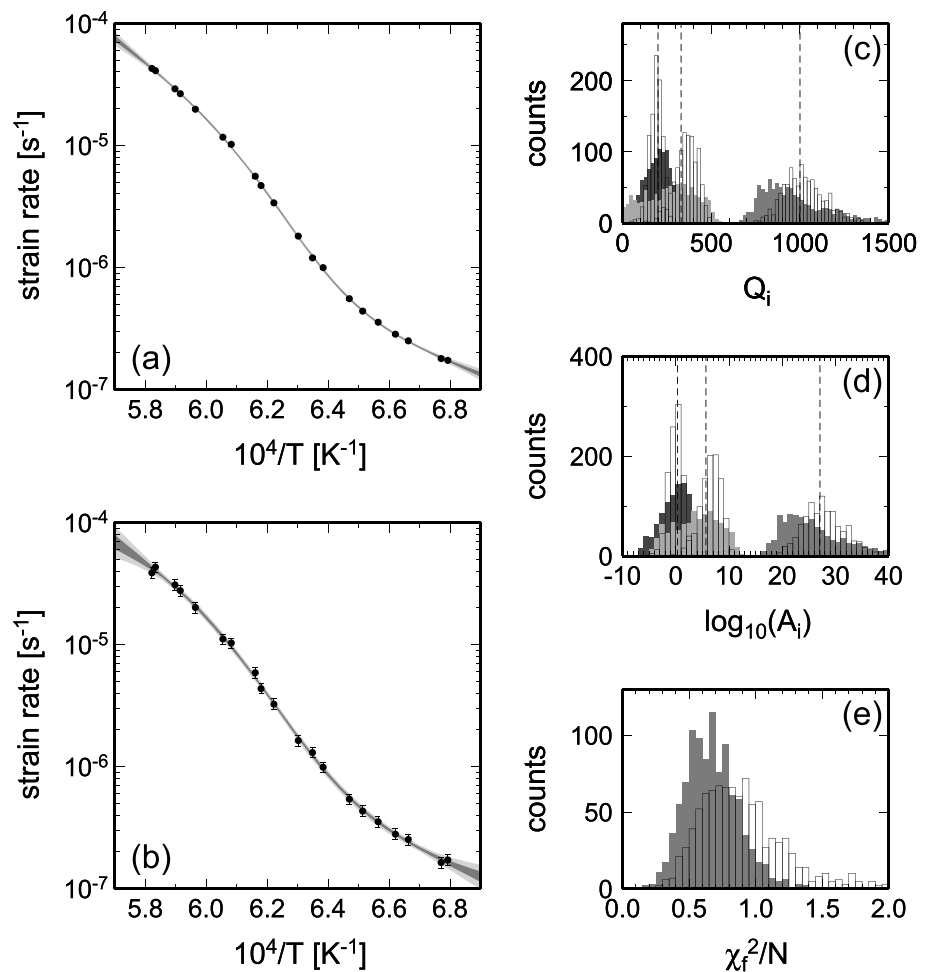


**Figure B4.** Similar to Figure B1 but for benchmark tests with variable-temperature data generated from the combination of parallel and sequential mechanisms.

Whereas the issue of parameter correlation has long been known among experimentalists, it is not common to report covariance or correlation coefficients even when multiple parameters are estimated jointly. Without covariance information, uncertainty associated with geological extrapolation cannot be evaluated in a meaningful manner.

Because the same stress component ( $n = 3.5$ ) is used for all flow laws of BMK91, the crossover of flow law predictions never occurs as stress varies. We note in passing that the flow laws of BMK91 for olivine single crystal have served as a foundation for the multiscale modeling of upper mantle plasticity and seismic anisotropy [e.g., Knoll *et al.*, 2009; Raterron *et al.*, 2014].

#### 6.4. Outlook

The comprehensive reanalysis of the experimental data of BMK91 helped to demonstrate the efficacy of the modified MCMC inversion algorithm and underscore the importance of joint inversion with interrater biases. Quite a few experimental studies on rock deformation have been published in the past two decades [e.g., Hirth and Kohlstedt, 1995a; Dimanov *et al.*, 1999; Mei and Kohlstedt, 2000; Bystricky and Mackwell, 2001; Xiao *et al.*, 2002; Stipp and Tullis, 2003; Rutter and Brodie, 2004; Li *et al.*, 2004; Hier-Majumder *et al.*, 2005; Rybacki *et al.*, 2006; Faul and Jackson, 2007; Raterron *et al.*, 2009; Mei *et al.*, 2010; Keefner *et al.*, 2011], and our plan is to revisit those which are most relevant to mantle dynamics, in a systematic manner. For example, KK08 estimated the stress exponent for the dry dislocation creep of olivine aggregates as  $\sim 5$ , whereas that for wet dislocation creep is  $\sim 3.6$ . The validity of this high exponent for dry dislocation creep remains to be investigated because of the aforementioned possibility of parameter bias in our previous inversion algorithm.

**Table C1.** Individual Inversion Results for  $\sigma$  Dependence

Run	$T$ ( $^{\circ}\text{C}$ )	$\sigma$ (MPa)	$f_{\text{O}_2}$ (atm)	Bai et al. [1991]		This Study	
				$\log_{10} A$	$n$	$\log_{10} A$	$n$
<i>[101]<sub>c</sub>, opx Buffer</i>							
7601	1400	20–53	$3.2 \times 10^{-5}$	$-10.1 \pm 0.2$	$3.4 \pm 0.1$	$-10.09 \pm 0.08$	$3.39 \pm 0.05$
7601	1400	29–84	$3.2 \times 10^{-10}$	$-12.0 \pm 0.2$	$4.0 \pm 0.1$	$-11.98 \pm 0.09$	$3.98 \pm 0.05$
<i>[101]<sub>c</sub>, mw Buffer</i>							
W504	1400	25–50	$2.0 \times 10^{-6}$	$-11.2 \pm 0.2$	$3.7 \pm 0.1$	$-11.16 \pm 0.10$	$3.73 \pm 0.07$
7602	1400	50–80	$3.2 \times 10^{-10}$	$-12.1 \pm 0.4$	$3.9 \pm 0.2$	$-12.10 \pm 0.20$	$3.88 \pm 0.11$
7602	1400	30–55	$7.9 \times 10^{-6}$	$-9.6 \pm 0.3$	$3.1 \pm 0.2$	$-9.61 \pm 0.12$	$3.11 \pm 0.08$
<i>[011]<sub>c</sub>, opx Buffer</i>							
5105	1400	100–120	$1.3 \times 10^{-7}$	$-14.8 \pm 1.2$	$4.7 \pm 0.6$	$-14.76 \pm 0.86$	$4.65 \pm 0.42$
5105	1400	85–115	$1.3 \times 10^{-4}$	$-13.9 \pm 0.8$	$4.5 \pm 0.4$	$-13.91 \pm 0.41$	$4.46 \pm 0.20$
5109	1400	80–120	$1.6 \times 10^{-7}$	$-13.9 \pm 0.4$	$4.1 \pm 0.2$	$-13.86 \pm 0.27$	$4.07 \pm 0.13$
7503	1400	80–133	$4.0 \times 10^{-5}$	$-15.0 \pm 0.9$	$4.9 \pm 0.4$	$-14.99 \pm 0.21$	$4.92 \pm 0.10$
7504	1400	100–175	$3.2 \times 10^{-10}$	$-12.0 \pm 0.2$	$3.3 \pm 0.1$	$-11.97 \pm 0.18$	$3.29 \pm 0.08$
7504	1400	59–115	$4.0 \times 10^{-5}$	$-10.9 \pm 0.2$	$3.1 \pm 0.1$	$-10.94 \pm 0.14$	$3.08 \pm 0.07$
<i>[011]<sub>c</sub>, mw Buffer</i>							
7501	1400	80–146	$3.2 \times 10^{-5}$	$-12.2 \pm 0.4$	$3.5 \pm 0.2$	$-12.23 \pm 0.15$	$3.52 \pm 0.08$
7501	1400	74–170	$3.2 \times 10^{-10}$	$-13.4 \pm 0.6$	$3.7 \pm 0.3$	$-13.34 \pm 0.21$	$3.65 \pm 0.10$
7502	1400	74–179	$3.2 \times 10^{-10}$	$-12.7 \pm 0.2$	$3.5 \pm 0.1$	$-12.73 \pm 0.11$	$3.46 \pm 0.05$
7502	1400	40–131	$3.2 \times 10^{-5}$	$-11.2 \pm 0.1$	$3.0 \pm 0.1$	$-11.18 \pm 0.09$	$2.99 \pm 0.05$
<i>[110]<sub>c</sub>, opx Buffer</i>							
S501	1400	25–40	$7.9 \times 10^{-7}$	$-9.7 \pm 0.4$	$3.0 \pm 0.3$	$-9.70 \pm 0.18$	$2.98 \pm 0.12$
W501	1400	20–45	$5.0 \times 10^{-9}$	$-9.9 \pm 0.2$	$3.1 \pm 0.1$	$-9.89 \pm 0.09$	$3.14 \pm 0.06$
7702	1260	51–102	$1.6 \times 10^{-7}$	$-11.3 \pm 0.2$	$3.4 \pm 0.1$	$-11.27 \pm 0.13$	$3.39 \pm 0.07$
7702	1350	24–63	$2.5 \times 10^{-7}$	$-10.2 \pm 0.1$	$3.3 \pm 0.1$	$-11.20 \pm 0.08$	$3.31 \pm 0.05$
<i>[110]<sub>c</sub>, mw Buffer</i>							
S502	1400	20–40	$2.5 \times 10^{-7}$	$-10.7 \pm 0.2$	$3.7 \pm 0.2$	$-10.73 \pm 0.12$	$3.68 \pm 0.08$
S504	1400	25–50	$5.0 \times 10^{-5}$	$-11.2 \pm 0.2$	$3.7 \pm 0.1$	$-11.16 \pm 0.10$	$3.73 \pm 0.07$
7703	1450	14–30	$1.6 \times 10^{-6}$	$-9.3 \pm 0.1$	$3.2 \pm 0.1$	$-9.31 \pm 0.09$	$3.19 \pm 0.07$
7703	1350	39–70	$1.0 \times 10^{-6}$	$-10.8 \pm 0.2$	$3.6 \pm 0.1$	$-10.84 \pm 0.15$	$3.55 \pm 0.09$

When exploring the effect of flow law parameter uncertainties on geodynamical models, it is of vital importance to take into account the parameter covariance. Perturbing a certain parameter independently to others is likely to violate the original experimental constraints from which flow law parameters were derived, though it has been a common exercise in modeling studies that use realistic rheology. *Alisic et al.* [2012], for example, explored the effect of the stress exponent  $n$  while fixing the scaling constant  $A$  and found that almost all aspects of their geodynamical models, including global plate motions, trench rollback, net rotation, plateness, and strain rate depend strongly on the stress exponent. In light of our discussion in section 6.3, the model sensitivity to the stress exponent is likely to be overestimated.

As noted by KK08, fully characterizing the uncertainty of flow laws (i.e., with covariance), if coupled with geodynamical modeling, could lead to useful feedback between rock mechanics and geodynamics. If we model mantle dynamics with an ensemble of perturbed flow laws, we would obtain a corresponding ensemble of modeling results. All of these models are compatible with relevant rock deformation data. The relation between flow law statistics and modeling statistics is likely to be strongly nonlinear, because mantle

**Table C2.** Individual Inversion Results for  $f_{O_2}$  Dependence

Run	$T$ (°C)	$\sigma$ (MPa)	Mechanism	Bai et al. [1991]		This Study	
				$\log_{10} A$	$m$	$\log_{10} A$	$m$
<i>[101]<sub>c</sub>, opx Buffer</i>							
7301	1500	30	1	$-3.1 \pm 0.1$	$0.3 \pm 0.1$	$-3.10 \pm 0.05$	$0.26 \pm 0.01$
7301	1425	40	1	-	$> 0.2$	$-3.83 \pm 0.04$	$0.19 \pm 0.01$
7301	1400	50	1	$-2.3 \pm 0.2$	$0.28 \pm 0.1$	$-3.15 \pm 0.28$	$0.20 \pm 0.02$
			2	$-4.05 \pm 0.2$	$0.05 \pm 0.03$	$-4.05 \pm 0.12$	$-0.01 \pm 0.05$
7301	1325	70	2	$-4.1 \pm 0.1$	$0.06 \pm 0.02$	$-4.09 \pm 0.05$	$0.06 \pm 0.01$
5202	1400	30	1	$-1.6 \pm 0.2$	$0.5 \pm 0.2$	$-1.40 \pm 0.36$	$0.51 \pm 0.04$
			2	$-4.8 \pm 0.1$	$0.1 \pm 0.1$	$-4.82 \pm 0.06$	$0.10 \pm 0.013$
5207	1400	50	1	$-2.0 \pm 0.1$	$0.3 \pm 0.3$	$-2.14 \pm 0.59$	$0.28 \pm 0.05$
			2	$-3.8 \pm 0.3$	$0.1 \pm 0.1$	$-3.34 \pm 0.07$	$0.13 \pm 0.03$
5215	1400	50	1	$-1.6 \pm 0.2$	$0.37 \pm 0.1$	$1.667 \pm 1.33$	$0.68 \pm 0.13$
			2	$-3.9 \pm 0.3$	$0.08 \pm 0.04$	$-3.64 \pm 0.06$	$0.15 \pm 0.01$
6104	1400	50	1	$-2.6 \pm 0.2$	$0.3 \pm 0.1$	$-2.01 \pm 0.66$	$0.30 \pm 0.05$
			2	$-4 \pm 1$	$0.1 \pm 0.1$	$-3.65 \pm 0.07$	$0.12 \pm 0.04$
6201	1400	50	1	$-1.5 \pm 0.1$	$0.4 \pm 0.1$	$0.43 \pm 1.61$	$0.55 \pm 0.16$
			2	$-3.9 \pm 0.1$	$0.08 \pm 0.03$	$-3.57 \pm 0.05$	$0.16 \pm 0.013$
6202	1400	50	1	$-2.3 \pm 0.1$	$0.3 \pm 0.1$	$-0.49 \pm 0.89$	$0.46 \pm 0.08$
			2	$-4.2 \pm 0.2$	$0.04 \pm 0.03$	$-3.94 \pm 0.06$	$0.11 \pm 0.014$
<i>[101]<sub>c</sub>, mw Buffer</i>							
W503	1400	50	1	$-0.658 \pm 0.1$	$0.565 \pm 0.2$	$-0.01 \pm 0.54$	$0.72 \pm 0.06$
			2	$-4.32 \pm 0.1$	$0.096 \pm 0.3$	$-4.97 \pm 0.05$	$0.13 \pm 0.01$
W504	1400	30	2	-	$< 0.18$	$-4.68 \pm 0.04$	$0.17 \pm 0.01$
5207	1400	50	1	$-1.7 \pm 0.1$	$0.4 \pm 0.1$	$-2.47 \pm 0.14$	$0.33 \pm 0.014$
			2	$-4 \pm 1$	$0.05 \pm 0.16$	$-4.16 \pm 0.15$	$-0.00 \pm 0.04$
5215	1400	50	1	$-2.3 \pm 0.1$	$0.4 \pm 0.1$	$-3.01 \pm 0.08$	$0.31 \pm 0.009$
			2	$-4 \pm 1$	$0.03 \pm 0.1$	$-4.68 \pm 0.11$	$-0.07 \pm 0.03$
6104	1400	50	1	$-2.5 \pm 0.1$	$0.3 \pm 0.1$	$-3.12 \pm 0.08$	$0.26 \pm 0.01$
			2	$-4 \pm 1$	$0.03 \pm 0.20$	$-4.44 \pm 0.13$	$-0.07 \pm 0.03$
6201	1400	50	1	$-2.1 \pm 0.1$	$0.41 \pm 0.1$	$-2.81 \pm 0.11$	$0.33 \pm 0.01$
			2	$-4.4 \pm 1$	$0.05 \pm 0.20$	$-4.67 \pm 0.14$	$-0.04 \pm 0.04$
<i>[011]<sub>c</sub>, opx Buffer</i>							
5101	1400	100	1	$-5.36 \pm 0.2$	$0.038 \pm 0.02$	$-5.80 \pm 0.42$	$-0.01 \pm 0.04$
			2	$-4.28 \pm 0.1$	$0.226 \pm 0.07$	$-4.21 \pm 0.12$	$0.23 \pm 0.04$
5212	1400	150	1	$-4.9 \pm 0.1$	$0.01 \pm 0.02$	$-4.75 \pm 0.39$	$0.04 \pm 0.03$
			2	$-3.9 \pm 0.1$	$0.20 \pm 0.07$	$-4.08 \pm 2.05$	$0.19 \pm 0.13$
5214	1400	150	1	$-4.99 \pm 0.1$	$0.019 \pm 0.02$	$-4.56 \pm 0.23$	$0.06 \pm 0.02$
			2	$-3.59 \pm 0.1$	$0.246 \pm 0.08$	$-3.23 \pm 0.28$	$0.37 \pm 0.09$
6101	1400	150	1	$-5.1 \pm 0.2$	$-0.01 \pm 0.03$	$-5.23 \pm 0.53$	$-0.02 \pm 0.05$
			2	$-3.6 \pm 0.1$	$0.20 \pm 0.07$	$-3.67 \pm 0.12$	$0.19 \pm 0.05$
6203	1400	150	1	$-5.0 \pm 0.4$	$0.03 \pm 0.06$	$-5.21 \pm 0.25$	$-0.01 \pm 0.02$
			2	$-3.6 \pm 0.1$	$0.3 \pm 0.1$	$-3.46 \pm 0.15$	$0.28 \pm 0.03$
<i>[011]<sub>c</sub>, mw Buffer</i>							
5104	1400	100	1	$-2.1 \pm 0.2$	$0.48 \pm 0.2$	$-3.10 \pm 0.12$	$0.37 \pm 0.01$
			2	$-5.607 \pm 1$	$-0.001 \pm 0.2$	$-5.74 \pm 0.07$	$-0.04 \pm 0.02$
5107	1400	100	1	$-2.7 \pm 0.2$	$0.4 \pm 0.1$	$-3.16 \pm -0.18$	$0.34 \pm 0.02$
			2	$-5 \pm 2$	$0.0 \pm 0.3$	$-5.55 \pm 0.11$	$-0.02 \pm 0.03$

**Table C2.** (continued)

Run	$T$ (°C)	$\sigma$ (MPa)	Mechanism	Bai et al. [1991]		This Study	
				$\log_{10} A$	$m$	$\log_{10} A$	$m$
<i>[011]<sub>c</sub>, mw Buffer</i>							
5110	1400	100	1	$-1.9 \pm 0.2$	$0.5 \pm 0.2$	$0.83 \pm 1.21$	$0.75 \pm 0.12$
			2	$-5 \pm 2$	$0.00 \pm 0.2$	$-4.80 \pm 0.09$	$0.14 \pm 0.02$
6203	1400	150	1	$-2.474 \pm 0.2$	$0.32 \pm 0.1$	$-2.93 \pm 0.40$	$0.25 \pm 0.04$
			2	$-4.648 \pm 0.7$	$0.0003 \pm 0.1$	$-4.48 \pm 0.05$	$0.03 \pm 0.03$
<i>[110]<sub>c</sub>, opx Buffer</i>							
S501	1400	30	3	-	$\sim 0.14$	$-4.40 \pm 0.05$	$0.14 \pm 0.01$
S502	1400	30	3	-	$\sim 0.14$	$-4.18 \pm 0.04$	$0.14 \pm 0.01$
W501	1400	30	3	-	$\sim 0.07$	$-4.84 \pm 0.05$	$0.07 \pm 0.01$
5206	1400	30	3	-	$\sim 0.13$	$-4.40 \pm 0.04$	$0.13 \pm 0.01$
5210	1400	30	3	-	$\sim 0.15$	$-4.13 \pm 0.04$	$0.15 \pm 0.01$
5213a	1400	30	3	-	$\sim 0.13$	$-4.05 \pm 0.05$	$0.13 \pm 0.01$
5213c	1400	30	3	-	$\sim 0.16$	$-3.86 \pm 0.05$	$0.16 \pm 0.01$
6103	1400	30	3	-	$\sim 0.13$	$-4.07 \pm 0.05$	$0.13 \pm 0.01$
6204	1400	30	3	-	$\sim 0.14$	$-3.86 \pm 0.05$	$0.14 \pm 0.01$
7203	1500	30	3	$-3.3 \pm 0.1$	$0.16 \pm 0.05$	$-3.31 \pm 0.07$	$0.16 \pm 0.01$
7204	1350	51	2	-	$< 0.18$	$-3.66 \pm 0.06$	$0.17 \pm 0.01$
7204	1300	50	2	$-5 \pm 3$	$0.1 \pm 0.1$	$-5.25 \pm 0.37$	$0.09 \pm 0.03$
			1	$-3.3 \pm 0.5$	$0.4 \pm 0.1$	$-3.34 \pm 0.12$	$0.35 \pm 0.33$
7205	1325	40	2	$-5.43 \pm 1$	$0.08 \pm 0.1$	$-5.50 \pm 0.48$	$0.08 \pm 0.04$
			1	$-3.705 \pm 0.1$	$0.31 \pm 0.1$	$-3.90 \pm 0.06$	$0.28 \pm 0.02$
7701	1240	80	2	$-5.508 \pm 2$	$0.05 \pm 0.2$	$-5.77 \pm 0.59$	$0.04 \pm 0.05$
			1	$-2.772 \pm 0.2$	$0.37 \pm 0.1$	$-3.24 \pm 0.09$	$0.30 \pm 0.02$
7701	1208	91	1	-	$> 0.28$	$-3.22 \pm 0.05$	$0.28 \pm 0.01$
<i>[110]<sub>c</sub>, mw Buffer</i>							
S501	1400	30	1&2	-	$\sim 0.18$	$-4.34 \pm 0.04$	$0.18 \pm 0.01$
S501	1400	30	1&2	-	$\sim 0.13$	$-4.55 \pm 0.04$	$0.13 \pm 0.01$
5201	1400	30	1&2	-	$\sim 0.08$	$-4.75 \pm 0.05$	$0.08 \pm 0.01$
5210	1400	30	1&2	-	$\sim 0.14$	$-4.87 \pm 0.04$	$0.14 \pm 0.01$
5213c	1400	30	1&2	-	$\sim 0.17$	$-4.28 \pm 0.04$	$0.17 \pm 0.01$
6103	1400	30	1&2	-	$\sim 0.14$	$-4.20 \pm 0.05$	$0.13 \pm 0.01$
6204	1400	30	1&2	-	$\sim 0.15$	$-4.62 \pm 0.05$	$0.15 \pm 0.01$
W504	1400	30	1&2	-	$\sim 0.17$	$-4.69 \pm 0.04$	$0.17 \pm 0.01$
7202	1500	30	2	$-3.01 \pm 0.2$	$0.23 \pm 0.08$	$-2.73 \pm 0.63$	$0.27 \pm 0.07$
			3	$-4.423 \pm 0.3$	$-0.02 \pm 0.04$	$-4.36 \pm 0.17$	$-0.01 \pm 0.05$
7206	1475	35	2	$-2.78 \pm 1$	$0.28 \pm 0.1$	$-2.46 \pm 0.56$	$0.32 \pm 0.08$
			3	$-4.33 \pm 0.4$	$-0.05 \pm 0.1$	$-4.30 \pm 0.09$	$-0.03 \pm 0.04$

dynamics itself is highly nonlinear. Which parameter uncertainty is most damaging is thus hard to predict. There may be, however, some model features that are persistent among the ensemble, and despite flow law uncertainties, certain modeling results may be claimed as robust. Conversely, other modeling features may be found highly variable, and in this case, the correlation between the flow law ensemble and the model ensemble should help us to identify the culprit flow law parameters. This type of “probabilistic” modeling could therefore delineate a subset of flow law parameters, the improvement of which by future experimental studies would have the highest impact on our understanding of geodynamics.

**Table C3.** Individual Inversion Results for  $T$  Dependence

Run	$\sigma$ (MPa)	$f_{O_2}$ (atm)	Mechanism	<i>Bai et al.</i> [1991]		This Study	
				$\log_{10} A$	$Q$ (kJ mol <sup>-1</sup> )	$\log_{10} A$	$Q$ (kJ mol <sup>-1</sup> )
<i>[101]<sub>c</sub>, opx Buffer</i>							
6302	50	$3.2 \times 10^{-10}$	1	-	< 340	$4.24 \pm 0.36$	$309 \pm 12$
6302	90	$3.2 \times 10^{-10}$	2	-	> 460	$10.8 \pm 0.34$	$481 \pm 10$
6302	70	$3.2 \times 10^{-10}$	1	$2.085 \pm 5$	$212 \pm 100$	$3.37 \pm 2.51$	$253 \pm 83$
			2	$19.66 \pm 2$	$760 \pm 250$	$19.6 \pm 4.21$	$755 \pm 124$
6401	70	$3.2 \times 10^{-10}$	1	$3 \pm 3$	$260 \pm 90$	$5.87 \pm 0.64$	$339 \pm 23$
			2	$16 \pm 1$	$660 \pm 220$	$18.8 \pm 4.75$	$719 \pm 139$
6403	50	$3.2 \times 10^{-5}$	2	-	>537	$12.3 \pm 0.31$	$542 \pm 10$
6403	50	$1.0 \times 10^{-9}$	1	-	<380	$5.86 \pm 0.31$	$356 \pm 10$
6403	50	$4.0 \times 10^{-4}$	2	-	>540	$12.6 \pm 0.40$	$560 \pm 12$
6406	50	$1.0 \times 10^{-9}$	1	-	<420	$7.43 \pm 0.30$	$412 \pm 10$
6406	50	$1.3 \times 10^{-5}$	2	-	>520	$11.6 \pm 0.30$	$526 \pm 10$
6407	70	$1.0 \times 10^{-9}$	1	-	<400	$7.04 \pm 0.31$	$381 \pm 10$
7101	50	$1.0 \times 10^{-8}$	1	$3.72 \pm 3$	$270 \pm 90$	$6.45 \pm 0.72$	$362 \pm 24$
			2	$16.15 \pm 1$	$660 \pm 220$	$22.2 \pm 4.86$	$835 \pm 145$
7102	50	$3.2 \times 10^{-5}$	2	-	>530	$12.5 \pm 0.37$	$548 \pm 12$
7103	50	$3.2 \times 10^{-10}$	1	-	<460	$8.52 \pm 0.37$	$442 \pm 12$
<i>[101]<sub>c</sub>, mw Buffer</i>							
W503	50	$3.2 \times 10^{-9}$	1	-	>400	$7.58 \pm 0.37$	$431 \pm 12$
6402	70	$3.2 \times 10^{-10}$	1	-	>59	$13.3 \pm 0.29$	$599 \pm 9$
6404	50	$1.3 \times 10^{-5}$	2	-	<430	$8.20 \pm 0.32$	$422 \pm 10$
6404	50	$1.0 \times 10^{-9}$	1	-	>490	$10.5 \pm 0.30$	$523 \pm 10$
6405	50	$1.0 \times 10^{-9}$	1	-	>620	$13.4 \pm 0.37$	$629 \pm 12$
6405	50	$1.3 \times 10^{-5}$	2	-	<452	$8.77 \pm 0.33$	$445 \pm 11$
7104	50	$3.2 \times 10^{-10}$	1	-	>500	$10.7 \pm 0.39$	$529 \pm 13$
7105	50	$1.3 \times 10^{-5}$	2	-	<450	$8.56 \pm 0.33$	$432 \pm 11$
7106	50	$2.5 \times 10^{-7}$	1	$18 \pm 2$	$730 \pm 240$	$14.6 \pm 2.65$	$625 \pm 80$
			2	$4 \pm 3$	$300 \pm 100$	$2.20 \pm 2.79$	$216 \pm 98$
7107	50	$2.5 \times 10^{-7}$	1	$16.45 \pm 1$	$680 \pm 230$	$26.3 \pm 6.02$	$968 \pm 180$
			2	$4.05 \pm 5$	$285 \pm 170$	$7.28 \pm 0.69$	$397 \pm 24$
<i>[011]<sub>c</sub>, opx Buffer</i>							
6601	150	$1.0 \times 10^{-9}$	1	-	~540	$11.3 \pm 0.39$	$537 \pm 13$
6602	100	$1.3 \times 10^{-5}$	2	-	~560	$11.8 \pm 0.36$	$558 \pm 12$
6602	100	$1.0 \times 10^{-9}$	1	-	~510	$10.1 \pm 0.38$	$513 \pm 12$
<i>[011]<sub>c</sub>, mw Buffer</i>							
6603	120	$1.3 \times 10^{-5}$	2	-	<500	$10.2 \pm 0.30$	$494 \pm 10$
6603	120	$1.0 \times 10^{-9}$	1	-	>630	$14.6 \pm 0.35$	$651 \pm 11$
7401	150	$3.2 \times 10^{-8}$	1	$19.13 \pm 1$	$760 \pm 250$	$21.4 \pm 2.57$	$825 \pm 76$
			2	$6.83 \pm 2$	$370 \pm 120$	$8.44 \pm 1.10$	$425 \pm 38$
7402	150	$3.2 \times 10^{-8}$	1	$18 \pm 1$	$730 \pm 240$	$16.3 \pm 1.71$	$676 \pm 50$
			2	$7 \pm 3$	$380 \pm 130$	$4.07 \pm 3.44$	$270 \pm 118$
<i>[110]<sub>c</sub>, opx Buffer</i>							
S502	30	$2.5 \times 10^{-7}$	3	-	<490	$0.24 \pm 2.41$	$157 \pm 80$
			2	-	>770	$20.8 \pm 0.94$	$826 \pm 28$
6301	30	$5.0 \times 10^{-7}$	3	-	<520	$10.1 \pm 0.41$	$495 \pm 13$
			2	-	>780	$40.8 \pm 1.87$	$1437 \pm 57$

**Table C3.** (continued)

Run	$\sigma$ (MPa)	$f_{O_2}$ (atm)	Mechanism	Bai et al. [1991]		This Study	
				$\log_{10} A$	$Q$ (kJ mol <sup>-1</sup> )	$\log_{10} A$	$Q$ (kJ mol <sup>-1</sup> )
<i>[110]<sub>c</sub>, opx Buffer</i>							
7201	30	$1.3 \times 10^{-5}$	3	-	<460	$9.19 \pm 0.32$	$450 \pm 10$
7203	30	$3.2 \times 10^{-10}$	3	-	<460	$8.53 \pm 0.39$	$450 \pm 13$
7203	46	$3.2 \times 10^{-10}$	3	$3.577 \pm 1$	$261 \pm 90$	$1.35 \pm 2.15$	$233 \pm 65$
			2	$28.87 \pm 4$	$1086 \pm 360$	$40.6 \pm 1.48$	$1447 \pm 47$
			1	$5.197 \pm 5$	$351 \pm 150$	$7.21 \pm 0.71$	$385 \pm 24$
7204	51	$3.2 \times 10^{-10}$	3	-	<410	$2.93 \pm 1.48$	$235 \pm 49$
			2	-	>830	$25.6 \pm 1.37$	$952 \pm 41$
7205	40	$2.5 \times 10^{-7}$	3	$5.68 \pm 1$	$330 \pm 110$	$6.49 \pm 1.09$	$377 \pm 31$
			2	$27.1 \pm 2$	$1000 \pm 300$	$37.7 \pm 4.42$	$1333 \pm 136$
			1	$0.318 \pm 2$	$200 \pm 70$	$8.18 \pm 1.82$	$418 \pm 60$
<i>[110]<sub>c</sub>, mw Buffer</i>							
5501	30	$4.0 \times 10^{-6}$	1	-	>700	$18.1 \pm 0.36$	$757 \pm 11$
6204	30	$2.5 \times 10^{-7}$	2	$6 \pm 9$	$400 \pm 300$	$-1.52 \pm 3.23$	$102 \pm 107$
			1	$30.4 \pm 1$	$1150 \pm 380$	$25.8 \pm 0.82$	$1008 \pm 25$
6204	80	$2.5 \times 10^{-7}$	1	-	~900	$24.5 \pm 0.38$	$919 \pm 12$
6501	30	$1.0 \times 10^{-9}$	2	-	<570	$11.3 \pm 0.37$	$548 \pm 12$
6501	30	$1.0 \times 10^{-5}$	2	$4 \pm 7$	$300 \pm 200$	$8.92 \pm 3.05$	$443 \pm 102$
			1	$26 \pm 2$	$980 \pm 330$	$26.6 \pm 5.52$	$993 \pm 166$
7202	30	$3.2 \times 10^{-6}$	2	$5.02 \pm 8$	$320 \pm 250$	$0.22 \pm 1.92$	$154 \pm 66$
			1	$25.15 \pm 0.7$	$970 \pm 320$	$20.8 \pm 0.76$	$836 \pm 23$
7206	30	$3.2 \times 10^{-5}$	2	$6.42 \pm 9$	$362 \pm 290$	$6.47 \pm 1.41$	$361 \pm 48$
			1	$22.19 \pm 1$	$847 \pm 280$	$19.0 \pm 2.06$	$752 \pm 60$

## Appendix A: Relative Variance due to Experimental Variables

The relative variance appearing in equation (2) may be calculated as

$$\begin{aligned}
 \text{rvar}(\{q_k\}; \{s_j^j\}) &= \frac{\text{var}(\dot{\epsilon}(\{q_k\}; \{s_j^j\}))}{(\dot{\epsilon}(\{q_k\}; \{s_j^j\}))^2} \\
 &\approx \frac{1}{(\dot{\epsilon}(\{q_k\}; \{s_j^j\}))^2} \sum_{i=1}^N \left( \frac{\partial \dot{\epsilon}}{\partial \dot{\epsilon}_i} \Big|_{q_k, s_j^j} \right)^2 \text{var}(\dot{\epsilon}_i(\{q_k\}; \{s_j^j\}))^2 \\
 &\approx \frac{1}{(\dot{\epsilon}(\{q_k\}; \{s_j^j\}))^2} \sum_{i=1}^N \left( \frac{\partial \dot{\epsilon}}{\partial \dot{\epsilon}_i} \Big|_{q_k, s_j^j} \right)^2 \left( \sum_{l=1}^L \left( \frac{\partial \dot{\epsilon}_i}{\partial s_l} \Big|_{q_k, s_j^j} \right)^2 \text{var}(s_l^j) \right), \quad (\text{A1})
 \end{aligned}$$

where  $N$  and  $L$  denote, respectively, the number of independent deformation mechanisms,  $\dot{\epsilon}_i$ , and the number of state variables (other than strain rate),  $s_l$ . The superscript  $j$  indexes data in an experimental run, signifying that this relative variance can be different for each datum, just as each strain rate can have different variance. The first-order Taylor expansion is used at each approximation above.

This relative variance measures the effect of the uncertainty of state variables such as temperature and stress on the uncertainty of predicted strain rate. It depends on flow law parameters,  $\{q_k\}$ , through  $\dot{\epsilon}$  itself and two kinds of partial derivatives. For an example with parallel mechanisms only, see KK08. When sequential mechanisms are involved, the first partial derivative becomes nontrivial.

## Appendix B: Results With Synthetic Data

In this section, we report results from single-run inversion with synthetic data. Four cases were prepared to test typical situations encountered when analyzing the data of BMK91. MCMC inversion was done with the

**Table D1.** Correlation Coefficients for Flow Law Parameters

<i>[101]<sub>c</sub> opx Buffer</i>												
	$n_1$	$Q_1$	$m_1$	$n_2$	$Q_2$	$m_2$	$B_1$	$B_2$				
$n_1$	1.0000	-0.4808	0.6195	0.2610	-0.6568	0.6064	-0.4555	-0.1959				
$Q_1$	-0.4808	1.0000	-0.6397	-0.6163	0.4845	-0.7834	-0.2233	0.5396				
$m_1$	0.6195	-0.6397	1.0000	0.6930	-0.7615	0.6930	0.4098	-0.6876				
$n_2$	0.2610	-0.6163	0.6930	1.0000	-0.4780	0.7102	0.5138	-0.9832				
$Q_2$	-0.6568	0.4845	-0.7615	-0.4780	1.0000	-0.7300	-0.1220	0.4313				
$m_2$	0.6064	-0.7834	0.6930	0.7102	-0.7300	1.0000	0.1463	-0.5877				
$B_1$	-0.4555	-0.2233	0.4098	0.5138	-0.1220	0.1463	1.0000	-0.5675				
$B_2$	-0.1959	0.5396	-0.6876	-0.9832	0.4313	-0.5877	-0.5675	1.0000				
<i>[101]<sub>c</sub> mw Buffer</i>												
	$n_1$	$Q_1$	$m_1$	$n_2$	$Q_2$	$m_2$	$B_1$	$B_2$				
$n_1$	1.0000	-0.1388	-0.1069	-0.2141	-0.1523	-0.2915	-0.6730	0.0502				
$Q_1$	-0.1388	1.0000	0.6684	-0.1964	0.3887	0.7216	0.5967	0.4719				
$m_1$	-0.1069	0.6684	1.0000	-0.2974	0.8201	0.8118	0.8033	0.5529				
$n_2$	-0.2141	-0.1964	-0.2974	1.0000	-0.2696	-0.1793	-0.0719	-0.8867				
$Q_2$	-0.1523	0.3887	0.8201	-0.2696	1.0000	0.7805	0.7072	0.5314				
$m_2$	-0.2915	0.7216	0.8118	-0.1793	0.7805	1.0000	0.8031	0.5965				
$B_1$	-0.6730	0.5967	0.8033	-0.0719	0.7072	0.8031	1.0000	0.3811				
$B_2$	0.0502	0.4719	0.5529	-0.8867	0.5314	0.5965	0.3811	1.0000				
<i>[011]<sub>c</sub> opx Buffer</i>												
	$n_1$	$Q_1$	$m_1$	$n_2$	$Q_2$	$m_2$	$B_1$	$B_2$				
$n_1$	1.0000	0.0313	0.2576	-0.2725	0.1109	0.2733	-0.4507	0.4031				
$Q_1$	0.0313	1.0000	0.4051	0.1697	-0.2577	0.3471	0.3505	-0.0720				
$m_1$	0.2576	0.4051	1.0000	0.4734	0.3873	0.8331	0.7432	-0.2534				
$n_2$	-0.2725	0.1697	0.4734	1.0000	0.3204	0.4742	0.6227	-0.9422				
$Q_2$	0.1109	-0.2577	0.3873	0.3204	1.0000	0.4278	0.2807	-0.2052				
$m_2$	0.2733	0.3471	0.8331	0.4742	0.4278	1.0000	0.5773	-0.1614				
$B_1$	-0.4507	0.3505	0.7432	0.6227	0.2807	0.5773	1.0000	-0.5082				
$B_2$	0.4031	-0.0720	-0.2534	-0.9422	-0.2052	-0.1614	-0.5082	1.0000				
<i>[011]<sub>c</sub> mw Buffer</i>												
	$n_1$	$Q_1$	$m_1$	$n_2$	$Q_2$	$m_2$	$B_1$	$B_2$				
$n_1$	1.0000	0.6812	0.6708	0.2327	0.4351	0.6862	-0.5095	-0.0155				
$Q_1$	0.6812	1.0000	0.7195	0.3630	0.1448	0.7501	-0.0189	-0.1359				
$m_1$	0.6708	0.7195	1.0000	0.5658	0.5746	0.7490	0.2919	-0.3885				
$n_2$	0.2327	0.3630	0.5658	1.0000	0.3225	0.4934	0.3735	-0.9332				
$Q_2$	0.4351	0.1448	0.5746	0.3225	1.0000	0.5506	0.1235	-0.1735				
$m_2$	0.6862	0.7501	0.7490	0.4934	0.5506	1.0000	0.0363	-0.1603				
$B_1$	-0.5095	-0.0189	0.2919	0.3735	0.1235	0.0363	1.0000	-0.4247				
$B_2$	-0.0155	-0.1359	-0.3885	-0.9332	-0.1735	-0.1603	-0.4247	1.0000				
<i>[110]<sub>c</sub> opx Buffer</i>												
	$n_1$	$Q_1$	$m_1$	$n_2$	$Q_2$	$m_2$	$n_3$	$Q_3$	$m_3$	$B_1$	$B_2$	$B_3$
$n_1$	1.0000	0.2585	-0.0847	-0.4521	0.0450	-0.0131	-0.0071	0.0006	0.0447	-0.8550	0.4798	-0.0043
$Q_1$	0.2585	1.0000	-0.2321	-0.3191	0.1563	-0.4087	-0.2017	-0.0790	-0.4189	0.1692	0.0895	-0.0079
$m_1$	-0.0847	-0.2321	1.0000	0.1040	-0.5454	-0.3339	-0.1224	-0.3156	-0.1505	0.2776	-0.3531	0.2292
$n_2$	-0.4521	-0.3191	0.1040	1.0000	0.0249	0.4705	-0.2571	0.1500	-0.1092	0.2964	-0.8067	0.2336
$Q_2$	0.0450	0.1563	-0.5454	0.0249	1.0000	0.2011	0.2772	0.7935	0.4467	-0.0956	0.3569	-0.3939
$m_2$	-0.0131	-0.4087	-0.3339	0.4705	0.2011	1.0000	-0.0963	0.2657	0.0551	-0.3169	0.0353	0.0661
$n_3$	-0.0071	-0.2017	-0.1224	-0.2571	0.2772	-0.0963	1.0000	0.3194	0.6368	-0.0990	0.3604	-0.9303

Table D1. (continued)

[110] <sub>c</sub> opx Buffer												
$Q_3$	0.0006	-0.0790	-0.3156	0.1500	0.7935	0.2657	0.3194	1.0000	0.5570	-0.1055	0.2585	-0.3904
$m_3$	0.0447	-0.4189	-0.1505	-0.1092	0.4467	0.0551	0.6368	0.5570	1.0000	-0.2671	0.3601	-0.4148
$B_1$	-0.8550	0.1692	0.2776	0.2964	-0.0956	-0.3169	-0.0990	-0.1055	-0.2671	1.0000	-0.5180	0.0400
$B_2$	0.4798	0.0895	-0.3531	-0.8067	0.3569	0.0353	0.3604	0.2585	0.3601	-0.5180	1.0000	-0.3584
$B_3$	-0.0043	-0.0079	0.2292	0.2336	-0.3939	0.0661	-0.9303	-0.3904	-0.4148	0.0400	-0.3584	1.0000
[110] <sub>c</sub> mw Buffer												
	$n_1$	$Q_1$	$m_1$	$n_2$	$Q_2$	$m_2$	$B_1$	$B_2$				
$n_1$	1.0000	-0.4294	-0.4832	-0.0061	-0.3252	-0.6101	-0.9590	-0.0570				
$Q_1$	-0.4294	1.0000	0.3982	0.0566	0.0452	0.5803	0.5486	-0.0530				
$m_1$	-0.4832	0.3982	1.0000	-0.0096	0.2106	0.0301	0.6963	-0.0564				
$n_2$	-0.0061	0.0566	-0.0096	1.0000	-0.6765	-0.0071	-0.0044	-0.9744				
$Q_2$	-0.3252	0.0452	0.2106	-0.6765	1.0000	0.1912	0.3326	0.7386				
$m_2$	-0.6101	0.5803	0.0301	-0.0071	0.1912	1.0000	0.5508	0.1539				
$B_1$	-0.9590	0.5486	0.6963	-0.0044	0.3326	0.5508	1.0000	0.0373				
$B_2$	-0.0570	-0.0530	-0.0564	-0.9744	0.7386	0.1539	0.0373	1.0000				

same setting in section 4. The a priori ranges are set as [1.0,6.0] for the stress exponents, [-0.1,1.0] for the oxygen fugacity exponents, and [0,1500] (in kJ mol<sup>-1</sup>) for the activation enthalpies. The maximum number of MCMC iterations is 10<sup>5</sup>, with  $D = 10$ ,  $P = 75$ , and  $C = 10$ , and the ensemble is resampled with an interval of 100.

The first case is with variable-stress runs (Figure B1). The assumed flow law is  $\dot{\epsilon} = A\sigma^n$ , with  $\log_{10} A = -12.1$  and  $n = 3.9$ . Two sets of synthetic data were generated, with the second set containing less accurate data than the first. Relative errors for stress and strain rate are, respectively, 1.4% and 3% for the first data set and 3% and 10% for the second set. The first data set yielded  $n = 3.89 \pm 0.09$  and  $\log_{10} A = -12.1 \pm 0.2$  and the second set  $n = 4.03 \pm 0.27$  and  $\log_{10} A = -12.3 \pm 0.5$ .

The second case is with variable-oxygen-fugacity runs (Figure B2). The assumed flow law is composed of two sequential mechanisms,  $\dot{\epsilon} = (A_1^{-1}f_{O_2}^{-m_1} + A_2^{-1}f_{O_2}^{-m_2})^{-1}$ , with  $\log_{10} A_1 = -1.6$ ,  $m_1 = 0.5$ ,  $\log_{10} A_2 = -4.9$ , and  $m_2 = 0.1$ . Again, two set of data were generated; relative errors for oxygen fugacity and strain rate are, respectively, 2% and 3% for the first data set and 2% and 10% for the second set. Inversion results are as follows:  $\log_{10} A_1 = -1.41 \pm 0.35$ ,  $m_1 = 0.52 \pm 0.03$ ,  $\log_{10} A_2 = -4.87 \pm 0.06$ , and  $m_2 = 0.11 \pm 0.01$  for the first set; and  $\log_{10} A_1 = -1.55 \pm 1.03$ ,  $m_1 = 0.50 \pm 0.10$ ,  $\log_{10} A_2 = -4.87 \pm 0.18$ , and  $m_2 = 0.10 \pm 0.04$  for the second set.

The third case is also with variable-oxygen-fugacity runs, but the assumed flow law is composed of two parallel mechanisms,  $\dot{\epsilon} = A_1 f_{O_2}^{m_1} + A_2 f_{O_2}^{m_2}$ , with  $\log_{10} A_1 = -5.4$ ,  $m_1 = 0.04$ ,  $\log_{10} A_2 = -4.3$ , and  $m_2 = 0.23$  (Figure B3). Two set of data were generated with the same relative errors as in the second case. Inversion results are as follows:  $\log_{10} A_1 = -5.47 \pm 0.49$ ,  $m_1 = 0.03 \pm 0.04$ ,  $\log_{10} A_2 = -4.24 \pm 0.18$ , and  $m_2 = 0.24 \pm 0.07$  for the first set; and  $\log_{10} A_1 = -5.20 \pm 0.48$ ,  $m_1 = 0.06 \pm 0.04$ ,  $\log_{10} A_2 = -3.78 \pm 0.82$ , and  $m_2 = 0.38 \pm 0.22$  for the second set.

The fourth case is with variable-temperature runs (Figure B4), and the assumed flow law is the combination of both parallel and sequential mechanisms:  $\dot{\epsilon} = A_1 \exp(Q_1/RT) + (A_2^{-1} \exp(-Q_2/RT) + A_3^{-1} \exp(-Q_3/RT))^{-1}$ , with  $\log_{10} A_1 = 0.32$ ,  $Q_1 = 200$  kJ mol<sup>-1</sup>,  $\log_{10} A_2 = 27.1$ ,  $Q_2 = 1000$  kJ mol<sup>-1</sup>,  $\log_{10} A_3 = 5.7$ ,  $Q_3 = 330$  kJ mol<sup>-1</sup>. Relative error for strain rate is 3% for the first data set and 10% for the second set. Temperature has an absolute error of  $\pm 1$  K for both sets. Inversion results are as follows:  $\log_{10} A_1 = -0.08 \pm 1.31$ ,  $Q_1 = 189 \pm 37$  kJ mol<sup>-1</sup>,  $\log_{10} A_2 = 27.9 \pm 3.9$ ,  $Q_2 = 1025 \pm 118$  kJ mol<sup>-1</sup>,  $\log_{10} A_3 = 6.57 \pm 1.93$ ,  $Q_3 = 359 \pm 64$  kJ mol<sup>-1</sup> for the first set, and  $\log_{10} A_1 = -0.05 \pm 2.67$ ,  $Q_1 = 190 \pm 75$  kJ mol<sup>-1</sup>,  $\log_{10} A_2 = 25.9 \pm 5.9$ ,  $Q_2 = 964 \pm 178$  kJ mol<sup>-1</sup>,  $\log_{10} A_3 = 3.89 \pm 4.18$ ,  $Q_3 = 270 \pm 139$  kJ mol<sup>-1</sup> for the second set.

In all of these four cases, the distributions of estimated flow law parameters encompass true values, and not surprisingly, the more accurate data sets exhibit better convergence to true values. Normalized  $\chi_f^2$  is  $\sim 1$  or lower, indicating that given data are explained within their uncertainty.

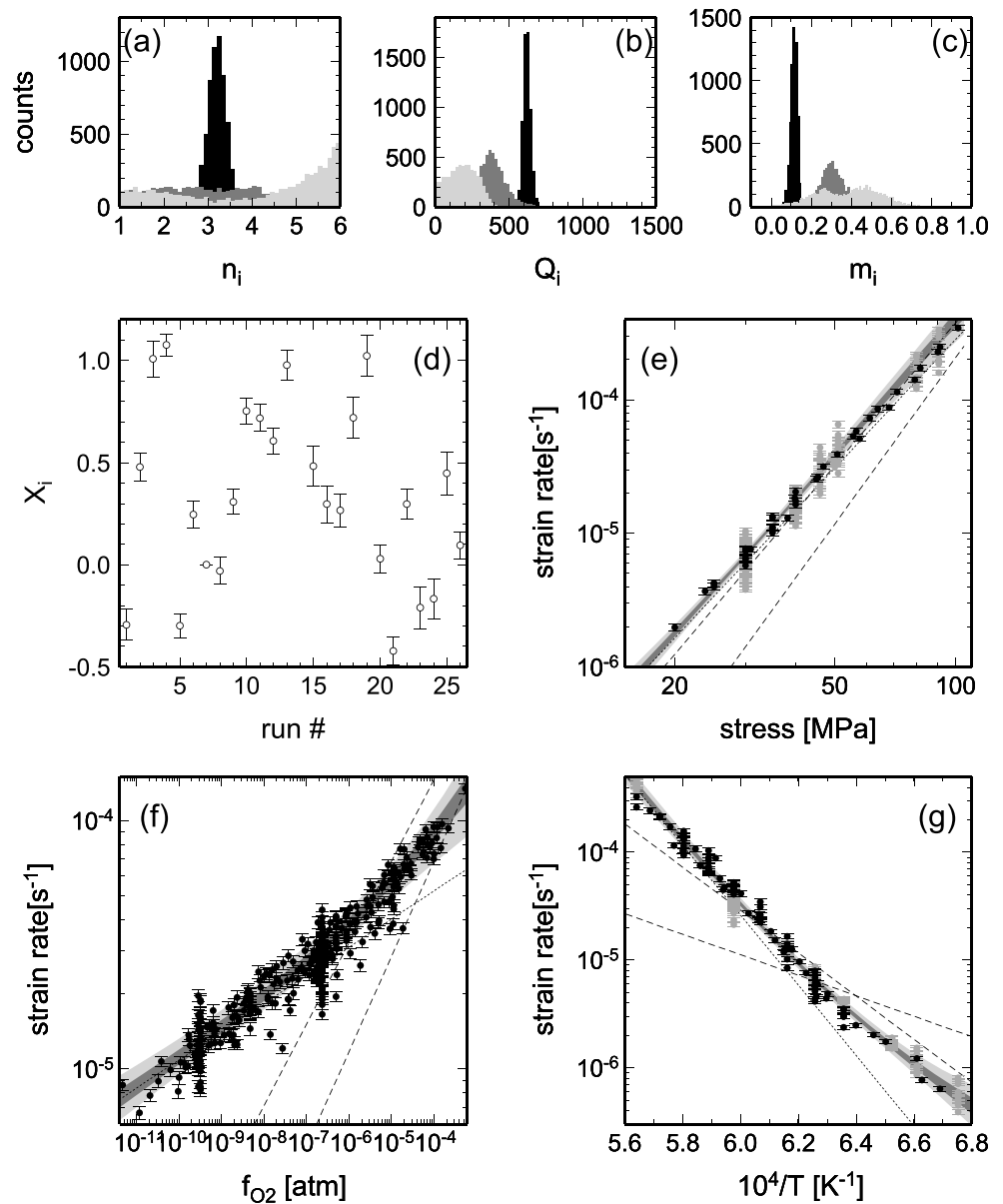


**Figure D1.** Same as Figure 12, with results based on the combination of parallel run numbers 1, 4, and 5 (Figure 13). The flow law parameters are as follows:  $n_1 = 3.20 \pm 0.21$ ,  $Q_1 = 623 \pm 25 \text{ kJ mol}^{-1}$ ,  $m_1 = 0.11 \pm 0.02$ ,  $A_1 = 16_{-8}^{+16}$ ,  $n_2 = 3.55 \pm 1.49$ ,  $Q_2 = 382 \pm 108 \text{ kJ mol}^{-1}$ ,  $m_2 = 0.33 \pm 0.11$ ,  $A_2 = 2.4_{-2.4}^{+450} \times 10^3$ ,  $n_3 = 4.14 \pm 1.65$ ,  $Q_3 = 182 \pm 97 \text{ kJ mol}^{-1}$ ,  $m_3 = 0.38 \pm 0.17$ , and  $A_3 = 1.0_{-1}^{+280} \times 10^{-4}$ .

### Appendix C: All Results for Individual Inversions

Results of single-run inversions are summarized in Table C1 for  $\sigma$  dependence, Table C2 for  $f_{O_2}$  dependence, and Table C3 for temperature dependence. The estimates of BMK91 are also listed for comparison.

### Appendix D: More Statistics for Joint Inversions

Correlation coefficients for estimated flow law parameters based on joint inversions are listed in Table D1.

The rejected results of joint inversion for the case of  $[110]_c$  with opx buffer are summarized in Figure D1.

### Acknowledgments

David Kohlstedt kindly provided information on the experimental uncertainty of BMK91. Comments by two anonymous reviewers were helpful to improve the clarity of the manuscript. All of experimental data analyzed in this study are available in Bai [1990]. Data of key inversion results are given in Table 2 as well as Tables C1–C3 and D1. This work was sponsored by the U.S. National Science Foundation under grant OCE-1417327.

### References

- Alisic, L., M. Gurnis, G. Stadler, C. Burstedde, and O. Ghattas (2012), Multi-scale dynamics and rheology of mantle flow with plates, *J. Geophys. Res.*, *117*, B10402, doi:10.1029/2012JB009234.
- Bai, Q. (1990), High-temperature creep of olivine single crystals, PhD thesis, Cornell Univ., Ithaca, New York.
- Bai, Q., S. J. Mackwell, and D. L. Kohlstedt (1991), High-temperature creep of olivine single crystals. 1, Mechanical results for buffered samples, *J. Geophys. Res.*, *96*, 2441–2463.
- Bystricky, M., and S. Mackwell (2001), Creep of dry clinopyroxene aggregates, *J. Geophys. Res.*, *106*, 13,443–14,354.
- Carter, N. L., and H. G. Ave Lallemand (1970), High temperature flow of dunite and peridotite, *Geol. Soc. Am. Bull.*, *81*, 2181–2202.
- Chen, S., T. Hiraga, and D. L. Kohlstedt (2006), Water weakening of clinopyroxene in the dislocation creep regime, *J. Geophys. Res.*, *111*, B08203, doi:10.1029/2005JB003885.
- Chopra, P. N., and M. S. Paterson (1984), The role of water in the deformation of dunite, *J. Geophys. Res.*, *89*, 7861–7876.
- Chu, X., and J. Korenaga (2012), Olivine rheology, shear stress, and grain growth in the lithospheric mantle: Geological constraints from the Kaapvaal Craton, *Earth Planet. Sci. Lett.*, *333–334*, 52–62.
- Dimanov, A., G. Dresen, X. Xiao, and R. Wirth (1999), Grain boundary diffusion creep of synthetic anorthite aggregates: The effect of water, *J. Geophys. Res.*, *104*, 10,483–10,497.
- Faul, U. H., and I. Jackson (2007), Diffusion creep of dry, melt-free olivine, *J. Geophys. Res.*, *112*, B04204, doi:10.1029/2006JB004586.
- Hansen, L. N., M. E. Zimmerman, and D. L. Kohlstedt (2011), Grain boundary sliding in San Carlos olivine: Flow law parameters and crystallographic-preferred orientation, *J. Geophys. Res.*, *116*, B08201, doi:10.1029/2011JB008220.
- Hier-Majumder, S., S. Mei, and D. L. Kohlstedt (2005), Water weakening of clinopyroxene in diffusion creep, *J. Geophys. Res.*, *110*, B07406, doi:10.1029/2004JB003414.
- Hirth, G., and D. Kohlstedt (2003), Rheology of the upper mantle and the mantle wedge: A view from the experimentalists, in *Inside the Subduction Factory*, edited by J. Eiler, pp. 83–105, AGU, Washington, D. C.
- Hirth, G., and D. L. Kohlstedt (1995a), Experimental constraints on the dynamics of the partially molten upper mantle: Deformation in the diffusion creep regime, *J. Geophys. Res.*, *100*, 1981–2001.
- Hirth, G., and D. L. Kohlstedt (1995b), Experimental constraints on the dynamics of the partially molten upper mantle: 2. Deformation in the dislocation creep regime, *J. Geophys. Res.*, *100*, 15,441–15,449.
- Jin, D., S. Karato, and M. Obata (1998), Mechanisms of shear localization in the continental lithosphere: Inference from the deformation microstructures of peridotites from the Ivrea zone, northwestern Italy, *J. Struct. Geol.*, *20*, 195–209.
- Karato, S. (2008), *Deformation of Earth Materials: Introduction to the Rheology of the Solid Earth*, Cambridge Univ. Press, Cambridge, New York.
- Karato, S., and H. Jung (2003), Effects of pressure on high-temperature dislocation creep in olivine, *Philos. Mag.*, *83*, 401–414.
- Karato, S., and P. Wu (1993), Rheology of the upper mantle: A synthesis, *Science*, *260*, 771–778.
- Karato, S., M. S. Paterson, and J. D. FitzGerald (1986), Rheology of synthetic olivine aggregates: Influence of grain size and water, *J. Geophys. Res.*, *91*, 8151–8176.
- Karato, S., H. Jung, I. Katayama, and P. Skemer (2008), Geodynamic significance of seismic anisotropy of the upper mantle: New insights from laboratory studies, *Annu. Rev. Earth Planet. Sci.*, *36*, 59–95.
- Keefner, J. W., S. J. Mackwell, D. L. Kohlstedt, and F. Heidelbach (2011), Dependence of dislocation creep of dunite on oxygen fugacity: Implications for viscosity variations in Earth's mantle, *J. Geophys. Res.*, *116*, B05201, doi:10.1029/2010JB007748.
- Knoll, M., A. Tommasi, R. E. Logé, and J. W. Signorelli (2009), A multiscale approach to model the anisotropic deformation of lithospheric plates, *Geochem. Geophys. Geosyst.*, *10*, Q08009, doi:10.1029/2009GC002423.
- Kohlstedt, D. L., B. Evans, and S. J. Mackwell (1995), Strength of the lithosphere: Constraints imposed by laboratory experiments, *J. Geophys. Res.*, *100*, 17,658–17,602.
- Korenaga, J., and S. Karato (2008), A new analysis of experimental data on olivine rheology, *J. Geophys. Res.*, *113*, B02403, doi:10.1029/2007JB005100.
- Li, L., D. Weidner, P. Raterron, J. Chen, and M. Vaughan (2004), Stress measurements of deforming olivine at high pressure, *Phys. Earth Planet. Inter.*, *143–144*, 357–367.
- Mei, S., and D. L. Kohlstedt (2000), Influence of water on plastic deformation of olivine aggregates: 1, diffusion creep regime, *J. Geophys. Res.*, *105*, 21,457–21,469.
- Mei, S., A. M. Suzuki, D. L. Kohlstedt, N. A. Dixon, and W. B. Durham (2010), Experimental constraints on the strength of the lithospheric mantle, *J. Geophys. Res.*, *115*, B08204, doi:10.1029/2009JB006873.
- Nishihara, Y., D. Tinker, T. Kawazoe, Y. Xu, Z. Jing, K. N. Matsukage, and S. Karato (2008), Plastic deformation of wadsleyite and olivine at high-pressure and high-temperature using a rotational Drickamer apparatus (RDA), *Phys. Earth Planet. Inter.*, *170*, 156–169.
- Raterron, P., E. Amiguet, J. Chen, L. Li, and P. Cordier (2009), Experimental deformation of olivine single crystals at mantle pressures and temperatures, *Phys. Earth Planet. Inter.*, *172*, 74–83.
- Raterron, P., F. Detrez, O. Castelnau, C. Bollinger, P. Cordier, and S. Merkel (2014), Multiscale modeling of upper mantle plasticity: From single-crystal rheology to multiphase aggregate deformation, *Phys. Earth Planet. Inter.*, *228*, 232–243.
- Robert, C. P., and G. Cassella (2004), *Monte Carlo Statistical Methods*, Springer, New York.
- Rubinstein, R. Y. (1981), *Simulation and the Monte Carlo Method*, John Wiley, New York.
- Rutter, E. H., and K. H. Brodie (2004), Experimental intracrystalline plastic flow in hot-pressed synthetic quartzite prepared from Brazilian quartz crystals, *J. Struct. Geol.*, *26*, 259–270.
- Rybacki, E., M. Gottschalk, R. Wirth, and G. Dresen (2006), Influence of water fugacity and activation volume on the flow properties of fine-grained anorthite aggregates, *J. Geophys. Res.*, *111*, B03203, doi:10.1029/2005JB003663.
- Sivia, D. S. (2006), *Data Analysis: A Bayesian Tutorial*, Oxford Univ. Press, New York.
- Skemer, P., J. M. Warren, L. N. Hansen, G. Hirth, and P. B. Kelemen (2013), The influence of water and LPO on the initiation and evolution of mantle shear zones, *Earth Planet. Sci. Lett.*, *375*, 222–233.
- Stipp, M., and J. Tullis (2003), The recrystallized grain size piezometer for quartz, *Geophys. Res. Lett.*, *30*(21), 2088, doi:10.1029/2003GL018444.
- Warren, J. M., and G. Hirth (2006), Grain size sensitive deformation mechanisms in naturally deformed peridotites, *Earth Planet. Sci. Lett.*, *248*, 438–450.
- Xiao, X., R. Wirth, and G. Dresen (2002), Diffusion creep of anorthite-quartz aggregates, *J. Geophys. Res.*, *107*(B11), 2279, doi:10.1029/2001JB000789.